The Study on the Effect of Mn Substitution in NaFeAs Superconductor

Azeb Shewafera

A Thesis Submitted to the Department of Applied Physics
School of Applied Natural Science
Presented in Partial Fulfillment of the Requirement
for the Degree of Masters in Physics (Material Physics)

Office of Graduate Studies
Adama Science and Technology University

July, 2021
Adama, Ethiopia

The Study on the Effect of Mn Substitution in NaFeAs Superconductor

Azeb Shewafera Irgete

Advisor: Dr. Mesfin Asfaw

A Thesis Submitted to the Department of Applied Physics
School of Applied Natural Science
Presented in Partial Fulfillment of the Requirement
for the Degree of Masters in Physics (Material Physics)

Office of Graduate Studies
Adama Science and Technology University

July, 2021
Adama, Ethiopia

Approval Page

I/we, the advisors of the thesis entitled **"The Study on The Effect of Mn Substitution in NaFeAs Superconductor"** and developed by Azeb Shewafera; hereby certify that the recommendation and suggestions made by the board of examiners are appropriately incorporated into the final version of the thesis.

Dr.Mesfin Asfaw _____ _____

Advisor Signature Date

We, the undersigned, members of the Board of Examiners of the thesis by Azeb Shewafera have read and evaluated the thesis entitled **"The Study on The Effect of Mn Substitution in NaFeAs Superconductor"** and examined the candidate during open defense. This is, therefore, to certify that the thesis is accepted for partial fulfillment of the requirement of the degree of Master of Science in Physics (Material Physics).

_____- _____ _____

Chairperson Signature Date

_____- _____ _____

Internal Examiner Signature Date

_____- _____ _____

External Examiner Signature Date

Finally, approval and acceptance of the thesis is contingent upon submission of its final copy to the Office of Postgraduate Studies (OPGS) through the Department Graduate Council (DGC) and School Graduate Committee (SGC).

_____- _____ _____

Department Head Signature Date

_____-	_____	_____
School Dean	Signature	Date
_____-	_____	_____
Office of Postgraduate Studies, Dean	Signature	Date

Declaration

I hereby declare that this Master Thesis entitled **"The study on the effect of Mn substitution in NaFeAs superconductor"** is my original work. That is, it has not been submitted for the award of any academic degree, diploma or certificate in any other university. All sources of materials that are used for this thesis have been duly acknowledged through citation.

Azeb Shewafera	_____	_____
Name of the Student	Signature	Date

Recommendation

I, the advisor of this thesis, hereby certify that I have read the revised version of the thesis entitled **"The study on the effect of Mn substitution in NaFeAs superconductor"** prepared under my guidance by **Azeb Shewafera** submitted in partial fulfillment of the requirements for the degree of Maters of Science in Physics(Material Physics). Therefore, I recommend the submission of revised version of the thesis to the department following the applicable procedures.

Mesfin Asfaw (PhD) _____ _____

Advisor Signature Date

ACKNOWLEDGEMENT

Above all, I would like to thank the almighty God; Next, I would like to give a deepest gratitude to my advisor and instructor Dr.Mesfin. for his guidance, assistance, contribution of valuable suggestions, more over I am heartily thankful for Dr.Mesfin who is a positive thinker who's every time civility thought me optimism. Finally, I would like to give a deepest gratitude to Adama Science and Technology University, School of Applied Natural Science, Department of Applied Physics program for providing me with a grant that helped me to carry out this work.

Table of Contents

List of Tables

List of Figures

List of Abbreviations

IBSC	Iron-Based Superconductors.
DFT	Density Functional Theory.
MRI	Magnetic Resonance Imaging.
BCS	Bardeen,Cooper, and Schrieffer theory.
ARPES	Angle Resolved Photoemission Spectroscope.
STM	Scanning Tunneling Microscopy.
NMR	Nuclear Magnetic Resonance.
SC	Superconductivity.
AFM	Antiferromagnetic.
SDW	Spin Density Wave.
DOS	Density of States.
FM	Ferromagnetic.
NM	Non-Magnetic.
CAFM	Collinear Anti Ferromagnetic.
DFT	Density Functional Theory.
BZ	Brillouin Zone.
HTS	High-Temperature Superconductors.
SQUID	Superconducting Quantum Interference Device.

TM	Transition Metal.
SCF	Self-Consistence Field.
CP	Car Parinello.
FPMD	First Principal Molecular Dynamics.
PWSCF	Plane Wave Self-Consistence Field.
ESPRESSO	opEn Source Package for Research in Electronic Structure, Simulation, and Optimization.

Abstract

This work present the study on the effect of Mn substitution in NaFeAs applying Density Functional Theory (DFT) as implemented in quantum ESPRESSO. The investigation of this effect were done, by 50% *Mn-substitution on Fe site of NaFeAs. The crystal structure of the NaFeAs and* $NaFe_{0.5}Mn_{0.5}As$ *were obtained. Convergence test were done. The band structure and the Density of State (DOS) are calculated for Non Magnetic (NM) and collinear-magnetic(Antiferomagnetic(AFM) and Feromagnetic (FM)) orderings. The calculated band structure and DOS adopt properties of other Iron Based Superconductors (IBSC). Comparison was done between NaFeAs and* $NaFe_{0.5}Mn_{0.5}As$*. The calculated band structures indicates that there is a significant change due to Mn-atom in AFM ordering, where the two bands are completely different at the first* Γ*-point and in between the second* Γ*-point and the first Z-point. There is double degeneracy nature of all bands along X-M and R-A points in NaFeAs at each orderings, but it decreases in the FM-ordering and Completely disappear in the AFM-ordering. The NaFeAs DOS result shows that the Fe states dominated in the vicinity of the fermi energy* E_F *with only a small contribution from the As and Na. But Mn and As shows dominance in the FM-*$NaFe_{0.5}Mn_{0.5}As$ *at and near Fermi-level. Using the DOS value and some approximation for BCS type, the Critical Temperature* T_c *were calculated and obtained to be* T_c *= 9.33 K for NaFeAs, and it is suppressed to 8.4 K for* $NaFe_{0.5}Mn_{0.5}As$ *in NM ordering. Mn substituted system also shows decrement of* T_c *in the FM(from 9.36 K to 9.1 K) and small enhancement in the AFM calculations. Concerning to the DOS in the AFM-NaFeAs has high DOS value.*

keywords: Superconductivity, Ferromagnetic, Antiferromagnetic, Quantum ESPRESSO.

1. Introduction

1.1 Background of the Study

Superconductivity is a phenomenon in which the resistivity of a material falls to zero when it is cooled at low temperature. Thus superconductivity (SC) is the absence of resistivity in solids those cooled below the transition temperature or critical temperature T_c. Thus zero resistivity is an essential characteristic of a superconductor [1]. In addition to this Superconductors have other unique property that is the ability to expel and screen magnetic fields [2].

Starting in 1911 when Kamerlingh Onnes discovery Superconductivity has an interesting history. Upon cooling elemental mercury to very low temperatures, the electrical resistance drops suddenly and vanished below a critical temperature of $T_c = 4.2K$ [15]. This resistanceless state is result in persistent currents to be produced in circuits to generate magnetic fields, and that store and transport energy without dissipation [16]. The discovery of Superconductor is not interrupted rather it becomes too wide after the 1911 study. So, over the intervening years many superconducting materials are discovered with higher critical temperatures [17], and are used into a number of technological applications such as MRI (Magnetic resonance imaging) systems for the health care industry [18].

In 1916, Silsbee, hypothesized the equality of a critical current for a superconducting wire to the current that produce the critical field at the surface of that wire. The reason for this behavior was made clear after the discovery of Meissner effect in 1933 [19]. The discovery was

continued and in subsequent decades other superconducting materials like metals, alloys and compounds were discovered. In 1941 niobium-nitride displayed superconductive property at $T_C = 16K$. In 1953 vanadium-silicon was found to superconduct at 17.5K. And, in 1962 the first commercial superconducting wire, an alloy of niobium and titanium (NbTi) were found. Not only was this, but the first widely-accepted theoretical understanding of superconductivity advanced in 1957 by American physicists John Bardeen, Leon Cooper, and John Schrieffer. Their theories of Superconductivity is named as the BCS theory derived from the first letter of each man's last name. The mathematically-complex BCS theory explained superconductivity at temperatures close to absolute zero for elements and simple alloys [20].

However, at higher temperatures and with different superconductor systems, the BCS theory has subsequently become inadequate to fully explain how superconductivity is occurring [21]. Another significant theoretical advancement came in 1962 when Brian D. Josephson, predicted that electrical current could flow between two superconducting materials even when they are separated by an insulator. This tunneling phenomenon was applied to electronic devices, like the superconducting quantum interference device (SQUID), and it is called "Josephson effect".

NaFeAs is the member of 111 family iron containing compounds. It appears to contain a superconductive order (in between 9-25 K) and magnetic order (below 45 K). NaFeAs adopts the tetragonal space group P4/nmm. Thus the crystal structure of this compound (a material that changes its behavior slightly) can exhibit superconductivity, magnetic property and metallic-conduction [10].

1.2 Statement of the Problem

Even though there are several models on the theory of high temperature superconductors (HTS), we have not found the one which would bring a good explanation of all physical properties at once. It is explained in many studies that NaFeAs is a superconductor under ambient

condition without impurity addition [11]. But it is known that impurity substitution may enhance superconductivity and in some compound magnetic impurities may suppress superconductivity, for instance it was reported that 0.2% Mn suppress superconductivity completely in $LaFe_{1-x}Mn_xAsO_{0.89}F_{0.11}$ [12]. Substitution of Mn atom in NaFeAs directly is not done yet. Thus we are initiated to study the effect of Mn atom substitution on the electronic structure of NaFeAs in our study, this idea being the problem of the study. Earlier studies reported that it is difficult to synthesize the compound NaFeAs experimentally, because of the loss of Na due to evaporation during the preparation of samples at high temperatures. That is NaFeAs and its doped variants are highly air-sensitive [13]. Moreover, a systematic investigation of various properties of this material is also very difficult [14]. Indeed Setup of laboratory experiments require materials, accurate devices and an environment fit experience, but this is expensive financially, spatially and it is time consuming until we get the results. So it was necessary to use simulation software, because it is inexpensive and requires less time and can be used for a good predictions. Thus Density functional theory (DFT) could be used to calculate the electronic structure of this compound computationally.

1.3 Objectives of the Study

1.3.1 General Objective of the Study

The general objective of this work was to study the effect of Mn Substitution in NaFeAs superconductor.

1.3.2 Specific Objectives of the Study

The specific objectives of this study were:

- to test the Convergence of plane wave cutoff (ecut) and BZ sampling (k-point)
- to obtain the band structure, the density of states and to study the magnetic property of $NaFe_{1-x}Mn_xAs(x = 0, 0.5)$
- to calculate the superconducting critical temperature.

1.4 Significance of the Study

This study was concerning about the effect of Mn Substitution in NaFeAs superconductor. It will be expected to have significant such as: raising public interest in the development of superconductors, contribution to acquire fundamental knowledge for better understanding of superconductor utilization, and furthermore It may help as a document for the future researchers those study on this area.

1.5 Limitation of the Study

Doing research is not such an easy task rather there are a lot of up and down (challenges). One of the faced problems is lack of large processor Computers.

1.6 Outline of the Thesis

In general, this thesis consists of five chapters. Each chapter will discuss on different issues related to the thesis. The first chapter describes an overview of the thesis background, statement of the problem, objective of the thesis, the significance of the study and Limitation of the study. Chapter two focuses on the review from previous studies that was made helpful to gain knowledge and to understand the thesis better. Chapter three gives description about the computational method in our study. Chapter four presents result and discussion. The last chapter five provide conclusions and recommendation.

2. Literature Review

2.1 General Overview of the Study

The phenomenon of superconductivity occurs in the phase space of three principal parameters [1]: temperature T, magnetic field B, and critical current density j. The critical temperature T_c is one of the first parameters that is measured and in a certain way defines the superconductor (it is the temperature at which a material changes from its normal to superconducting state). Critical magnetic field is a field beyond which the superconductor returns to its ordinary state. And critical current is the current which form magnetic field to changes the state of the superconductor.

Although there are materials those superconducts at low temperatures without any impurity addition, this superconductive behavior can be suppressed by adding some impurities. For example, the undoped parent compounds like, LaFePO, LiFeAs, and FeSe, are nonmagnetic and superconducting even without doping. In contrast, undoped LaFeAsO and $BaFe_2As_2$, are non-superconducting antiferromagnetic metals, and electron or hole doping may suppresses the magnetic order and induces superconductivity [3].

After the addition of magnetic impurities the state of the superconductor may be changed to a magnetic state. That is many superconducting materials belong to families of compounds that can be tuned into or out of superconductivity by one or more tuning parameters [4]. The

superconducting state often does not appear in the parent compound under ambient conditions, even at extremely low temperature. Single crystalline $BaFe_2As_2$ undergoes strongly coupled tetragonal to orthorhombic and paramagnetic to antiferromagnetic phase transitions at 134 K but it does not super conduct under ambient conditions all the way down to 2 K. These coupled structural and magnetic transitions can be suppressed by application of mechanical pressure. Thus mechanical pressure as well as a subset of these chemical substitutions can also induce superconductivity [4].

While we compar between Superconductivity and Magnetism Superconductivity is formed due to Cooper pairs of electrons, mostly being diamagnetic because of spin singlet state, but Magnetism is generated due to long range ordering of a complex particle having electrical charge and an electron spins. So, the relationship between magnetism and superconductivity had been estimated to be ambivalent. The use of magnetic elements, like Fe, Ni and Co, was intentionally avoided so far in the area of superconductivity. But, the discovery of HTS (high temperature superconductors) based on iron significantly initiated research in this field [5].

To study the behavior of the materials their electronic structures can be used . There are many ways (methods) to calculate these structures. Density Functional Theory (DFT) [6] can be mentioned among the methods. The electronic structures of a superconductor can be calculated using DFT as implemented by the computer program known as Quantum ESPRESSO [7]. And pseudo potential approximation is used for electronic band structure calculation, for determination of density of states, Fermi energy, total energy, and electronic structure along high symmetric directions.

The band structure of a materials provide the range of energies that an electron within the materials can have and ranges of energy it can not have (band gaps). The band structure provide the way in which energies of the state's are changed with a 3D vector k which is common to plot the energies along the high-symmetry points. The energies along high-symmetry directions represent the maximum and minimum energies for the bands around all Brillouin

zone(BZ). Although the band structure explain the crystal lattice nature, along high symmetry points, it is not a reliable guide, because it only explain the bands about high symmetry points. An energy below or above which all states may be occupied is called the Fermi energy. If many band-structures are shifted the Fermi energy is at zero,unless the Fermi energy will may be marked clearly [8].

The density of state (DOS) is one of the electronic structure which is the number of different states in the particular energy range allowed to be occupied by electrons. The calculation of DOS depends on the full density of states over the whole Brillouin zone. But it does not depend on special directions unlike the band structure. The BZ should be sampled just as for the calculation of the ground state. Computing a band structure or a DOS may be simple, if the imputes are prepared well and the ground state density is computed with a good k-point values. If the density is fixed for the band structure/DOS calculation it may be a lot quicker than the ground state calculation but it may have more k-points. While one should look for a superconductor with the highest possible DOS near the Fermi-energy in a superconductor shows a strong electron-phonon interaction via, a hybridization of electron states around the Fermi level [9].

2.2 BCS (Bardeen, Cooper and Schrieffer) Theory

The BCS theory is a successful microscopic explanation for the conduction in superconductivity [22]. It could quantitatively predict the properties of a superconductor. This theory is based on the formation of pairs of electrons of momenta k and -k with one electron spin up and the other spin down, proposed by Leon Cooper, which shows that there is instability of the Fermi surface at the ground state upon the formation of pairs of 'bound' state electrons. This bound pairs of electrons are attracted to each other via the electron-phonon interaction and it is also known as the Cooper pairs. The zero resistance in superconductivity can be explained by the movement of these Cooper pairs through the lattice unaffected by the thermal

vibrations. This is because at low temperatures, the attractive phonon interactions between the electrons are stronger than the interaction between the electrons and ions. Hence, the electron-phonon interactions overcome the Coulomb interaction.

2.3 Classification of Superconductors

According to Nicholas Gerbis superconductors are classified in to two types depending on how they react in a magnetic field. These are: Type I and Type II superconductors. Type I superconductor is usually made of pure metal. When it is cooled below its critical temperature it exhibits zero resistivity and displays perfect diamagnetism. This means that the magnetic fields cannot penetrate it while it is in the superconducting state. Type II: These superconductors are usually alloys and their diamagnetism is more complex. All superconductors have a critical magnetic field. This is the field that either makes or breaks its superconducting state. Type I superconductors change states of matter once at one threshold. Type II superconductors can change states twice at two different magnetic field thresholds. This is important because of what is known as the Meissner effect. Which is the reason why superconductors can levitate permanent magnets. The superconductor doesn't allow the magnetic field to penetrate it. It actually mirrors the field. This is what causes the levitation. Type I superconductors always have the Meissner effect. Type II superconductors can get caught between their magnetic field thresholds and partially allow magnetic fields to permeate them causing flux [23]. This is shown in the figure 2.1.

Conventional superconductivity refers to electron-phonon-coupled superconducting electron pairs described by BCS theory. Unconventional superconductivity refers to superconductors where the Cooper pairs are not bound together by phonon exchange but instead by exchange of some other kind, for example spin fluctuations in a superconductor with magnetic order either coexistent or nearby in the phase diagram. Since the discovery of unconventional SC in the layered cuprates in 1986, the study of these materials saw T_c jump to 164 K by 1994. Further progress in high-temperature SC would be aided by understanding the cause

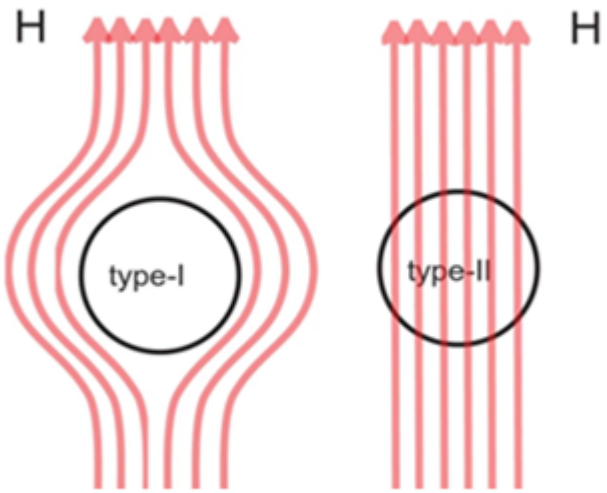

Figure 2.1: Type I and Type II superconductors [24].

of such unconventional pairing. The first superconductor identified as unconventional was $CeCu_2Si_2$, T_c = 0.6K, reported by Steglich et al. In 1979 Rather than electron-phonon coupling, the pairing in $CeCu_2Si_2$ has been described as due to some sort of fluctuations either quantum critical or antiferromagnetic(AFM) [25]. The Steglich et al.'s discovery led to the discovery of other unconventional superconductors of the same class as shown in Figure 2.2(A schematic view stating briefly about the history of superconductors that have been discovered so far).

2.4 Critical Temperature of Superconductor

The critical temperature for superconductor is the temperature at which the electrical resistivity of a metal drops to zero [26]. The transition is so sudden and complete that it appears to be a transition to a different phase of matter; this superconducting phase is described by the BCS theory. Several materials exhibit superconducting phase transitions at low temperatures.

The temperature below which a sample is superconducting in the absence of a magnetic field is called the critical temperature, T_c. At any given temperature, $T < T_c$, there is a certain minimum field $B_c(T)$, called the critical field, which will kill superconductivity. It is found (experimentally and theoretically) that B_c is related to T by the equation:

$$B_C = B_0\left(1 - \left(\frac{T}{T_c}\right)^2\right) \tag{2.1}$$

Where, B_0 is the asymptotic value of the critical field as $T \to 0K$.

The highest critical temperature was about 23 K until the discovery in 1986 of some high temperature superconductors. Materials with critical temperatures in the range 120 K have received a great deal of attention because they can be maintained in the superconducting state with liquid nitrogen (77 K). And now a days HTS (High Temperature Superconductor)is approaching to the room temperature. Figure 2.2 shows the discovery of some superconductors with their transition temperature.

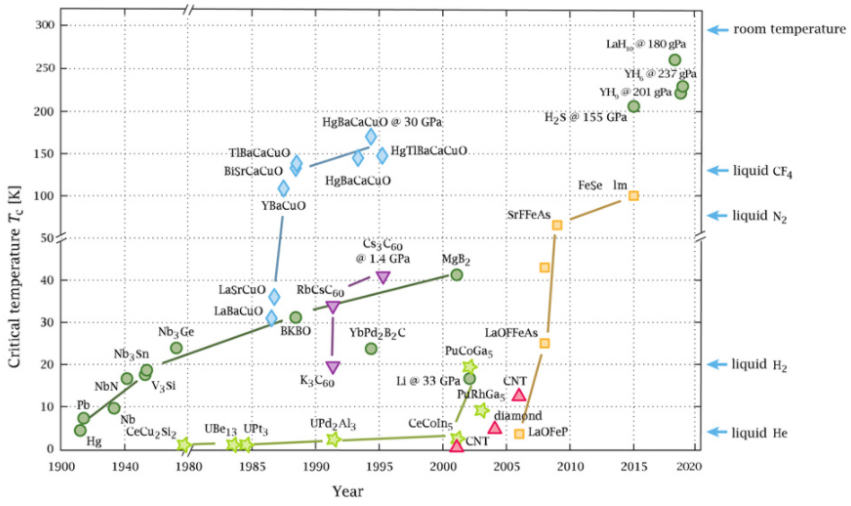

Figure 2.2: A brief histories of Superconductors and their T_c [28].

The theory of superconductivity is accurate and well developed and that, given certain properties of the normal state of a given metal. Superconducting properties like T_c can be calculated with accuracy. The necessary properties of the normal state are: the electron energy bands near the Fermi energy, the phonon dispersion curves, the fully screened electron-phonon interaction matrix elements, and the fully dressed Coulomb interaction between electrons. All these properties are not sufficiently well known for any metal to make first-principles calculation of its superconducting properties worthwhile. There is much to be learned, however, by approaching the problem from the other direction and asking what can be learned about the normal metal from its measured superconducting properties.

There are available for a number of superconducting metals and alloys measurements of the superconducting transition temperature T_c, the Debye temperature Θ_D, and the electronic heat capacity coefficient γ. Also, for a few metals, there are measurements of the phonon energies and of the isotope shift of T_c. By making use of theoretical formula for T, and experimental data, one can find empirical values for electron-phonon coupling constant λ and the phonon enhancement of cyclotron mass and specific heat. The measured isotope shifts can be used to find empirical values for the Coulomb coupling constant μ^*. With the addition of information about the phonon energies, we will be able to examine the makeup of λ and discuss the in influence of the various metallic properties upon the variations of λ throughout the periodic table. Finally, it will be pointed out that the theory makes a reasonably definite statement about the maximum T_c that one should expect for a given class of materials.

Thus for a specific superconductor the microscopic parameters such as the average phonon frequency, Θ_D (the average phonon frequency, wich is expressed in degrees Kelvin), the electronic density of states, $N(E_F)$, etc are needed to estimate T_c of a superconductor. According to the strong-coupling formula T_c is expressed by:

$$T_c = \frac{\Theta_D}{1.45} exp\left(- \frac{1.04(1+\lambda)}{\lambda - \mu^*(1+0.62\lambda)} \right) \tag{2.2}$$

This equation is known as the MacMillans Formula. Where μ^* is the Coulomb pseudopotential parameter, usually given by:

$$\mu^* = 0.13\frac{N(E_F)}{1+N(E_F)} \tag{2.3}$$

2.5 Iron Based Superconductors (IBSCs) and Their History

Iron-based superconductors (IBSC) are iron-containing chemical compounds whose superconducting properties were discovered since 2006 [3]. The primary IBSC is LaFePO which superconduct with T_c = 4K in 2006. In 2008, led by recently discovered iron pnictide compounds [29] (originally known as oxypnictides). They were in the first stages of experimentation and implementation for which T_c jumped to 26K for the doped $LaFeAsO_{1-x}F_x$ (found by Hosono's group in January 2008) [30]. This innovation rekindled global interest in this area and opened a new frontier for superconductivity. Although in the early stage this superconductor family was called 'Pnictide Superconductors', researchers now call them 'Iron based Superconductors' (IBSC) because several measurements and evaluations have clarified that they all have similar electronic structure where the 3d electrons derived from Fe ion play an important role in superconductivity. The appearance of iron chalcogenide affects also to call IBSC [31].

Previously most high-temperature superconductors were cuprates and being based on layers of copper and oxygen sandwiched between other substances (La, Ba, Hg)) [32]. This new type of superconductors is based instead on conducting layers of iron and a pnictide (chemical elements in group 15 of the periodic table, here typically arsenic (As) and phosphorus (P)) and seems to show promise as the next generation of high temperature superconductors. Much of the interest is because the new compounds are very different from the cuprates and may help lead to a theory of non-BCS theory superconductivity [33]. More recently these have been called the ferropnictides [34]. The first ones found belong to the group of oxypnictides. Unlike high-T_c copper-oxide superconductors, electronic structures and magnetic properties

of iron-based superconductors are quite well understood. Since electron-phonon interaction is too weak to explain the superconducting transition temperature as high as 55 K, the iron-based superconductors provide an excellent chance to understand an unconventional superconductivity which might be helpful to reveal the origin of high-T_c superconductivity in copper oxides [35].

Iron is a typical magnetic element with a large magnetic spin moment, and had been believed to the most harmful for emergence of superconductivity. However, the situation was totally changed since the discovery of an iron oxypnictide superconductors $LaFeAsO_{1-x}F_x$ with T_c=26K [35]in early 2008. This discovery sparked intense research activity on superconductivity in this system as a consequence, many papers have been published to date along with several comprehensive review articles and monographs.

Iron-based superconductors has impacts, like, the breaking of a widely accepted belief that "iron is antagonistic against superconductivity", which led to the opening of a versatile frontier in superconducting materials. It has become clear through intense research and so far researchers shows that iron can be a good friend for high T_c-superconductors under certain conditions [36]. The other is a rich variety in candidate materials and in pairing interaction. IBSCs have several unique properties such as robustness to impurity, high upper critical field and excellent grain boundary nature. These properties are advantageous for wire application. Recent progress in the performance of superconducting wires of IBSC is wide eyed, that is the maximal critical current has reached the level of commercial metal-based superconducting wires.

2.6 IBSCs in Contrast with Cuprates

Study of iron based superconductors and their physical properties have been one of the major activities in condensed matter physics in the past several years. At the time when the iron

based superconductor was discovered, scientists in the field of SC were well prepared. Several powerful new techniques such as angle resolved photoemission spectroscope (ARPES), scanning tunneling microscopy (STM), have been well developed during the course of studying high T_c cuprates. These techniques together with some more conventional techniques such as neutron scattering, nuclear magnetic resonance (NMR), optical conducting measurements, have been applied to examine the properties of the new compounds. Iron based SC shares many common features with the high T_c cuprates. Both of them are unconventional superconductors in the sense that phonons unlikely play any dominant role in their SC. Both are quasi-two dimensional, and their SC is in the proximity of AFM.

On the other hand, iron based superconductors have a number of distinct properties from the cuprates. The parent compounds of the SC cuprates are AFM Mott insulators due to strong Coulomb repulsion, and the lightly doped superconductors are doped Mott insulators. On the other hand, the parent compounds of iron based superconductors are semi metallic. Dynamic mean field calculations indicate that the iron based compounds are close to metal-insulator transition line but are at the metallic side [37]. In the curpates, the low energy physics is described by a single band [38] while in the iron-based compounds, there are multi orbitals involved. Despite over long years of study, some of the physics in the cuprates remain controversial. The investigation of iron based superconductors may help us to understand the unconventional SC and also provide a new route for searching higher temperature superconductors [39].

2.7 The Effect of Impurity in IBSCs

Impurity substitution in a given parent compound may affect the state of the system. It has been reported that adding impurity can change magnetic property, or structural property, or other properties of the material. Thus the superconducting compound may be changed its

property in to magnetic, insulating or other properties or may not be changed. This behavioral change depends on the properties of the impurity which is substituted in the given compound. For instance the transition-metal (TM) elements (such as Co or Ni) are widely used to achieve SC by substituting the iron ions [40]. However, this substitution is significantly different from that of other doped materials, because the TM ions enter the conducting planes and may also act as the impurities. Likewise magnetic impurities may introduce magnetic properties. In general, the magnetic impurity induces the magnetic pair-breaking effect and, resultantly, larger T_c suppression than that by the nonmagnetic impurity in the first two class of IBSCs [41]. But, not only the presence of impurity can give rise to SC. That is there are compounds those can superconduct without addition of impurity. As it was mentioned in chapter one LaFePO, LiFeAs and FeSe are superconductors under ambient conditions without doping whereas LaFeAsO and $BaFe_2As_2$ can't superconduct before doping [42].

2.7.1 The Effect of Mn Atom in Iron Based Superconductors

The suppression of T_c by impurity adding is dependent on the impurity elements, and the Mn substitution strongly destabilizes the superconductivity in the first two class of IBSCs. The Mn acts as a magnetic impurity in this system. This fact reveals that T_c is suppressed by the pair-breaking effect of the magnetic moments of Mn. In general, the magnetic impurity may induces the magnetic pair-breaking effect and, resultantly, larger T_c suppression than that by the nonmagnetic impurity.

For instance adding Mn atom in $FeTe_{0.5}Se_{0.5}$, $BaFe_2As_2$, $Na(Fe_{0.97-x}Co_{0.03}Mn_x)$, and $Na_{1-\delta}(Fe_{1-x}Mn_x)$As suppresses the transition temperature. In $Fe_{1-x}Mn_xTe_{0.5}Se_{0.5}$ due to the presence of Mn atom (doping) T_c decrease [43]. Likewise in a Single crystal Ba122, $Ba(Fe_{1-x}Mn_x)_2As_2$, as x increases from zero up to $x = 0.1$ the structural and magnetic phase transition temperature is suppressed. For $x > 0.1$, a resistive feature associated with magnetic ordering is observed with a transition temperature that increases with x. Superconductivity is not observed for any value of x. The suppression of structural temperature and enhancement of magnetic temperature occurs at a slower rate for Mn [44]. But if the value of x increases the rate of suppression

occurs rapidly. For example, P. F. S. Rosa et al.in 2014 shows that on substitution of Mn in $BaFe_2As_2$ superconductor for $BaFe_{1.9}Mn_{0.1}As_2$ this single crystals display very low SC transition temperature (T_c) and no Superconductivity [45].

Additionally $Ba(Fe_{1-x}Mn_x)_2As_2(x = 0.08)$, which fails to become a superconductor. With decreasing temperature, a transition from the paramagnetic phase to the antiferromagnetic phase was clearly observed by angle-resolved photoemission spectroscopy. The absence of superconductivity in $Ba(Fe_{1-x}Mn_x)_2As_2$ can be ascribed both to the absence of carrier doping in the FeAs plane and to the stabilization of the antiferromagnetic order by the Mn impurities. Likewise Mn doping gives magnetic impurities, and can enhance the residual resistivity and suppress the superconductivity in the case of $Na(Fe_{0.97-x}Co_{0.03}Mn_x)$. The suppression of T_c gets much weaker beyond $x = 0.03$ and superconductivity survives even up to a residual resistivity of $2.86m\Omega cm$ [46]. In a single crystals of $Na_{1-\delta}(Fe_{1-x}Mn_x)As$ a non-superconducting phase down to 1.8 K is achieved by formal hole doping when Fe is substituted by Mn in NaFeAs along with the formation of a magnetic phase. This magnetic phase has also strong impact on the material properties. Doping with Mn on the Fe site as formal hole doping strongly affects the properties since all phase transitions of the parent compound are absent, where magnetization and resistivity exhibit strikingly different temperature dependencies. [47].

2.7.2 Magnetic Transitions in IBSC Family

For the superconducting state, the impurity scattering effect is closely related to the gap structure, the characteristics of the impurities and the underlying electronic structure. The impurity scattering effect may give some important clues as regards how to unravel the pairing gap structure as well as the pairing mechanism [48, 1]. According to Anderson's theorem, in a conventional superconductor a magnetic impurity can break the Cooper pairs easily, while superconductivity is retained robustly with the presence of nonmagnetic impurities in the

unitary limit [49]. In sharp contrast, Anderson's theorem is violated for unconventional superconductors, where both magnetic and nonmagnetic impurities are detrimental to superconductivity [46].

The undoped parent compounds of iron-based superconductors are either superconducting or antiferromagnetic at low temperatures. As it was mentioned above LaFePO, LiFeAs, and FeSe, for example, are nonmagnetic and superconducting under ambient conditions even without doping. In contrast, undoped LaFeAsO and $BaFe_2As_2$, are non-superconducting antiferromagnetic metals, and electron or hole doping suppresses the magnetic order and induces superconductivity [50, 51]. The undoped 1111-type iron pnictides show structural and magnetic phase transitions at slightly different temperatures. With electron or hole doping, the antiferromagnetic order in some compounds is suppressed and superconductivity emerges [51].

In $BaFe_2As_2$, the systematic replacement of either the alkaline-earth metal (Ba), transition metal (Fe), or pnictogen (As) with different elements almost universally suppresses the non-superconducting antiferromagnetic state of parent compounds to a superconducting nonmagnetic state. This phase transition from the antiferromagnetic state to the superconducting state is generic property of the iron-based superconductor systems which can also be produced by applied external pressure. It is remarkable that the phase diagram of the iron-based superconductor system is very similar to that of copper-oxide materials except that the undoped parent compound of copper-oxide materials is an antiferromagnetic [52]. The pair-breaking effect by Co-doping overcomes the development of superconductivity derived from the suppressed, fluctuating SDW, leading to the characteristic physical properties in Co-doped 122 [53].

2.8 NaFeAs

NaFeAs is a member of the 111 family IBSCs which provide different properties at different conditions. At ambient temperature it is in a tetragonal phase, but upon cooling it undergoes a structural tetragonal-to-orthorhombic structural transition at around 54K, and at 45K, and 9-25 K, corresponding to, magnetic and superconducting transitions, respectively [54, 55]. Below $T = 10K$ non-bulk superconductivity arises, coexisting with magnetism in the orthorhombic phase [56]. NaFeAs appear to be the only iron pnictides which superconduct at ambient pressure next to LiFeAs when Fe is formally in the +2 oxidation state [57, 58, 59]. As NaFeAs contains Fe ions, in a near-perfect tetragonal environment, seemingly the optimal crystallographic condition for superconductivity, it is possible that by modifying the electron count by doping Tc may be enhanced. NaFeAs adopts the tetragonal space group P4/nmm. The crystal structure of NaFeAs is similar to that of LiFeAs and it is given in figure 2.3. The band structure and DOS of NaFeAs shows the same properties to the rest IBSC, and they are shown in figure 2.4.

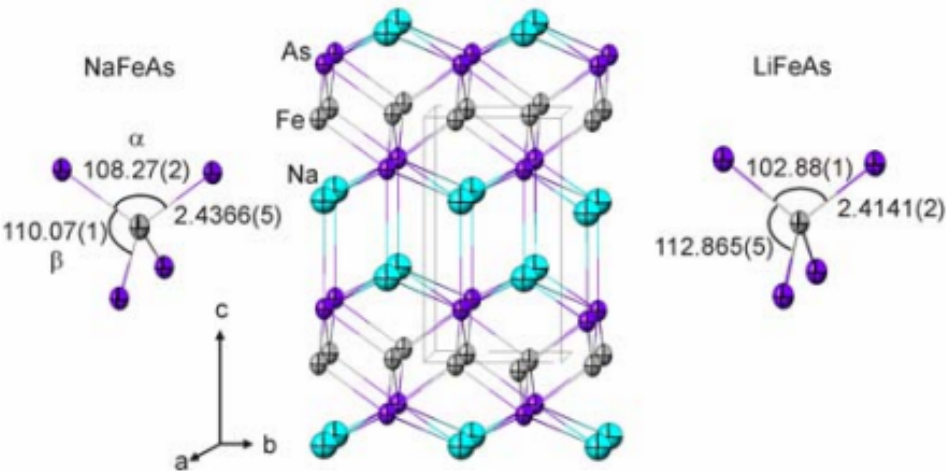

Figure 2.3: Crystal structure of NaFeAs [57].

Moreover, it was reported that no magnetic order is detected at all temperatures in 111 family, whereas the spin-density wave (SDW) state has been found in the 1111 and 122 type Fe-based

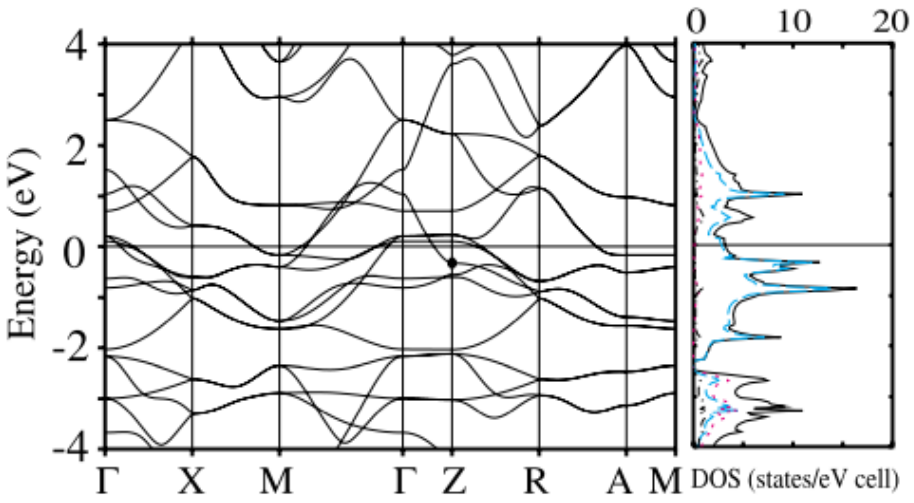

Figure 2.4: Band structure and DOS of NaFeAs [60].

superconductors. The absence of SDW transition and the relatively low T_c in comparison with the 1111 and 122 type parent compounds make the 111 families a possible candidates for being conventional BCS superconductors [61]. But this is not true for all 111 family IBSCs, that is although the T_c values for "111" type superconductors are much lower than those for the other two types of iron arsenide superconductor, they are too high to be accounted by sole electron-phonon coupling [62]. It means that its superconducting mechanism cannot be explained by conventional BCS theory. In some sense, NaFeAs is significant with regards to examining the superconducting mechanism in the Fe-based superconductor field. It is noticeable that the stoichiometric NaFeAs compound is difficult to be synthesized by experiment, because of the evaporation loss of Na during the high temperature. Relation with the fast development of computer; first-principles calculations become a powerful tool to study the ground state properties. For instance R. A. Jishi and H. M. Alyahyaei in 2009 studied electronic structure and lattice vibrational frequencies of LiFeAs and NaFeAs by means of DFT calculations [60].

Stoichiometric NaFeAs showed a 10% superconducting volume fraction and long-range AFM ordering in most of its volume. These results imply that there might be some overlap between

the AFM ordered and superconducting regions in the phase diagram in this material [63]. Indeed NaFeAs is a superconductor under ambient conditions even without any impurity addition, the substitution of Pd and Ni for Fe in NaFeAs which formally corresponds to electron doping suppresses the structural and magnetic phase transition completely and enhances the superconducting volume fraction. On the other hand, doping with Cr and Mn as formal hole doping strongly affects the properties since all phase transitions of the parent compound are absent, where magnetization and resistivity exhibit strikingly different temperature dependencies. Bulk magnetic order seems to be established in the Cr-doped case. In contrast to the Ba-122 family, Ni and Pd dopings yield different physical properties in NaFeAs [47]. In 1111 series, Mn doping has been shown to suppress superconductivity and to add additional strong scattering centers [64]. On other hand if 50% Cu is substituted in the Fe of NaFeAs ($NaFe_{0.5}Cu_{0.5}As$) it resides in a crossover regime between Mott-type and Slater-type insulating behavior, and strong electronic correlations are essential for realizing its insulating state [65].

Charge doping and hydrostatic pressure modify superconductivity in the 111 systems. Substitutions of Fe by Co, Ni and Cu have been achieved in NaFeAs they destroy the magnetic order and enhance T_c up to a maximum around $5-6\%$ in electron doping. The effect of pressure in NaFeAs, for which T_c gets enhanced at lower values of pressure (while long-range magnetic order gets destroyed) up to $33Kat \sim 4GPa$ getting reduced and eventually vanishing at higher values of pressure. While we compere these effects with in the other 111 families of superconductors like LiFeAs and LiAsP, substitutions of Fe by Co, Ni and Cu are detrimental for superconductivity in the case of LiFeAs, for LiFeP, no doped samples have been synthetized so far. But unlike which in NaFeAs in LiFeP and LiFeAs, T_c gets reduced for increasing pressure until it vanishes at $\sim 3GPa$ and $\sim 10GPa$ respectively, being the T_c of LiFeAs always higher [62].

Electronic correlation could be suppressed in this compound by applying either the chemical pressure or doping electrons but not by doping holes [66]. In similarity to other iron-based superconductors, the density of states in the vicinity of the Fermi energy is found to be

dominated by contributions from the Fe 3d states in NaFeAs and the electron-phonon coupling parameter value is found to be too small to account for the superconducting transition temperatures. This shows that iron-based superconductors are not of the conventional type, where the attractive electron-electron interaction is mediated by phonons [56]. The SDW ordering of NaFeAs is greatly enhanced upon pressure. It also shows a fluctuating feature of the SDW ordering in an intermediate temperature below TSDW, which may be caused by thermal fluctuations of domain walls, and high-temperature incommensurability [67].

2.9 Density Functional Theory

Density functional theory (DFT) is a computational quantum mechanical modeling method used in physics, chemistry and materials science to investigate the electronic structure (or nuclear structure) or principally the ground state of many-body systems, in particular atoms, molecules, and the condense phases [68]. DFT is the First principles method to study the ground state of many-body systems. Using this theory, the properties of a many-electron system can be determined by using functional, that is functions of another function. DFT is among the most popular and versatile methods available in condensed-matter physics, computational physics, and computational chemistry. DFT can be applied as implemented by the computer program known as Quantum ESPRESSO [69].

This theory was introduced by Walter Kohn around 1965. For inventing this powerful technique he was awarded the Nobel prize in 1998. DFT is a commonly used method in science to describe properties of condensed matter systems [13]. DFT is a useful method to understand and predict the properties of many materials. This method allows studying materials even with minimum input parameter like the atomic type and lattice parameters, and that is why it is also called first principle method.

DFT is a type of electronic structure calculation that has rapidly gained popularity. That is DFT is very successful in describing structural and electronic properties in materials science

and chemical science. It approaches any interacting problem by mapping it exactly to a non-interacting problem that gives an alternative way to tackle the problem. According to the Hohenberg, Kohn, 1964 explanation "Every observable quantity of a quantum system can be calculated only from the density of the system" [70]. The density of particles interacting with each other can be calculated as the density of an auxiliary system of non-interacting particles as it was explained by Kohn, Sham, in 1965. Thus DFT is a ground-state theory in which the charge density is the relevant physical quantity. It was so challenge to approximate functional and computational cost. In 1990's there are widely used functional that give a quite reasonable accuracy with the affordable computational cost.

2.9.1 Hohenberg-Kohn Theorem

There are two parts in this theorem. One states that the ground state energy is uniquely depends on the electron density (It is a functional of electron density) [70]. If the ground state density is $\rho(r)$, the total energy is E, hence according to this theory, all properties of a many-body system can be determined by the ground state charge density as:

$$E = E[\rho(r)] \tag{2.4}$$

The ground state energy E is also uniquely determined by the ground-state charge density $\rho(r)$ (the density that minimizes the total energy is the exact ground state density). Thus, by minimizing the energy of the system according to the electron density, ground state energy can be obtained.

$$E(\rho) = E_0[\rho_0(r)] \tag{2.5}$$

where E_0 is the minimum energy, $\rho_0(r)$ is the initial charge density

Thus H-K only provides that there exists one-to-one mapping relations between electron density functional and system properties. But they do not give any about what exactly these relations are. So, instead of the minimizing the system energy, the Kohn-Sham method is most generally used.

2.9.2 The Kohn-Sham Equations

Kohn and Sham system is a feasible way to utilize the H-K model to solve the electrons systems by mapping interacting system to non-interacting system. In 1965, Kohn and Sham showed that it is possible to reduce the many-body quantum mechanical problem to an exactly equivalent set of one-electron equations, solved self-consistently. This is a reformulation of the following idea. The system of interacting electrons is mapped on to an auxiliary system of non-interacting electrons having the same ground state charge density $\rho(r)$ [71]. In Kohn-Sham equation the Schrodingers equation for the system is give in the form of:

$$[\frac{\hbar^2}{2m}\nabla^2 + V(r) + V_H(r) + V_{XC}(r)]\Phi_i(r) = \varepsilon_{(i)}\Phi_i(r) \tag{2.6}$$

where: $V(r)$ is the external potential acting on the interacting system, $V_H(r)$ is the Hartree (or Coulomb) potential, $V_{XC}(r)$ is the exchange correlation potential and Φ_i is the wave function.

Calculating the Kohn-Sham equation is not as straightforward as it is expected. It is must to follow the following stapes to do this calculation. First to find the ground state energy we need the electron density, so to find the electron density we need to solve the equation and find the wave function, but to find the wave function we need to have the total potentials, and for finding the potentials we need to have the electron density. So, as we see we are trapped in a loop that to find one thing we need another thing. But: First, we put the positions of the atom and guess the electron density ($\rho_{in}(r)$) as the atoms are not interacting with each other. Then by this electron density we find the potential. After that we find the wave function($\Phi_i(r)$) And by this wave function we can calculate the new electron density ($\rho(r)$). If the new electron density is as the same as the previous electron density, we keep it and calculate the energy.

If not, using this electron density and we must go to the second step. The diagram of this self-consistence field is given in figure 2.5.

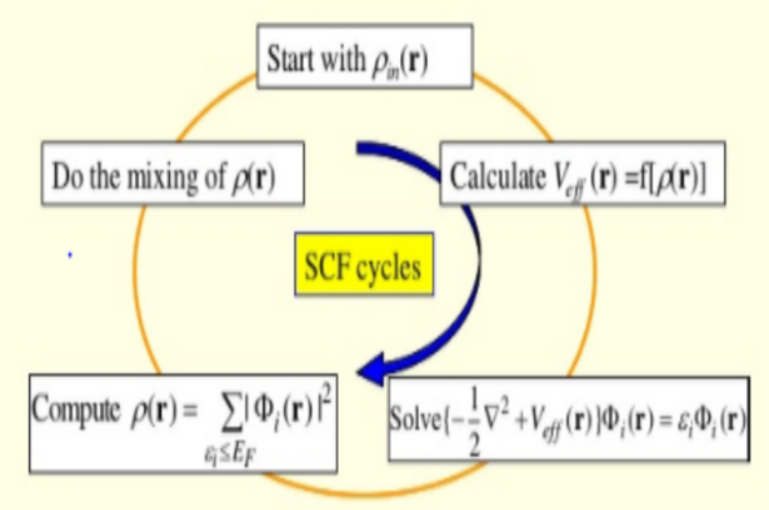

Figure 2.5: Self-consistent field (SCF)cycle. [72]

2.10 Quantum ESPRESSO

Quantum Espresso is software (a computational technique) which is used for first principle calculation of periodic and disordered systems based on DFT. That is it depends on electron-ion interaction, electron-electron interaction, plane wave and pseudo potentials to calculate the ground state and Kohn sham orbitals of materials. This software has components like plane wave self-consistence field (PWSCF) which is method to calculate the phonon dispersions for complex materials, that is to study the stability of crystal. The electronic structures can be calculated by expanding the wave functions into plane waves, car parinello (CP), and first principal molecular dynamics (FPMD) [73].

Quantum ESPRESSO stands for opEn Source Package for Research in Electronic Structure, Simulation, and Optimization. It is freely available to researchers around the world under the terms of the General Public License. Quantum Espresso builds upon newly restructured

electronic structure codes that have been developed and tested by some of the original authors of novel electronic-structure algorithms and applied in the last two decades by some of the leading materials modeling groups worldwide. Innovation and efficiency are still its main focus, with special attention paid to massively-parallel architectures, and a great effort being devoted to user friendliness. Quantum ESPRESSO is evolving towards a distribution of independent and inter-operable codes in the spirit of an open-source project, where researchers active in the field of electronic structure calculations are encouraged to participate in the project by contributing their own codes or by implementing their own ideas into existing codes [74].

3. Methodology

We have used Density Functional Theory (DFT) to carry out this study. DFT is among the most popular and versatile methods available in condensed-matter physics, computational physics, and computational chemistry to investigate the electronic structure or nuclear structure (principally the ground state) of many-body systems, in particular atoms, molecules, and the condense phases [75]. Using this theory, the properties of a many-electron system can be determined by using functional, that is Functions of another function [76], which in this case are the specially dependent on electron density.

DFT is applied in this study as it was implemented by the computer program known as Quantum ESPRESSO. And we have used pseudo potential approximation for electronic structure calculation for determination of density of states, Fermi energy, total energy, and electronic structure along high symmetric directions. We have look for different pseudopotentials from quantum ESPRESSO home page (We have downloaded the suitable pseudopotentials for Na, Fe, As and Mn from alternative pseudopotential library in order to obtain high quality and meaningful results). We have done magnetic and non magnetic ordering calculations.

The band structures were calculated along highs symmetric direction in the conventional tetragonal Brillion zone, the lattice following the path,$\Gamma - X - M - \Gamma - Z - R - A - Z$, as shown in the figure 3.1. We have used grace software to plot the band structure and DOS, and XCrySDen software to draw the crystal structures of NaFeAs and $NaFe_{0.5}Mn_{0.5}As$.

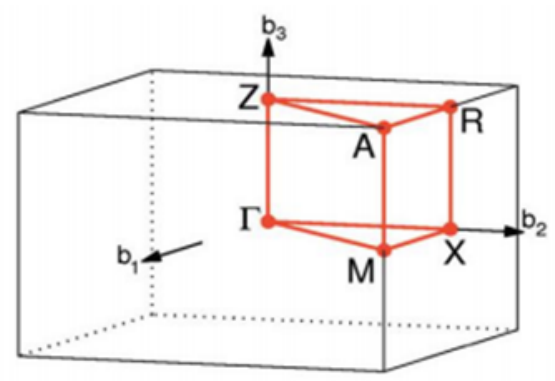

Figure 3.1: Brillouin zone of TFT with path: $\Gamma - X - M - \Gamma - Z - R - A - Z$ [77].

The crystal structure of NaFeAs has tetragonal structure with the space group P4/nmm. To obtain the structures the tetragonal initial lattice parameters in our calculations are based on the experimental value. Thus in the input preparation of basic self-consistent (scf) calculation we have used an experimental value for the lattice parameters, a = b = 3.924[a.u] and c = 6.919[a.u] [78], and the values for the K-point mesh were 8 8 5 in our calculation. Then we did a vc-relax calculations (optimization of cell parameters). Using the optimized cell parameters we did each calculations (calculations for the scf, band and DOS). We found the K-points for the calculation of the band using the XCrySDen software. We have used the smearing occupation for the scf and band calculations, and tetrahedral occupation for the density of state (DOS) calculation.

The relationship between magnetism and superconductivity has been one of the most discussed topics in iron-based superconductors, thus we did both nonmagnetic and magnetic calculations. First we did nonmagnetic calculations and then we did collinear magnetization calculations. That is Ferromagnetic(FM) and antiferromagnetic(AFM) calculations. We make a fixed magnetization 0.5 Bohr magneton, by checking the value which is at stable energy level. We also did the projection calculation (projwfc calculation) for each DOS.

4. Result and Discussion

4.1 Crystal Structure and Total Energy

In this chapter we present the results obtained from Density Functional Theory Calculation with Quantum Espresso. Using the methods mentioned in chapter three, we did basic self-consistent field (scf) calculation, Convergence of plane waves cutoff (ecut), Convergence of BZ sampling (k-point), Lattice constant optimization (vc-relax Calculation) for a good preparation of imputes. The graph of total energy Versus plane wave cutoff is given in figure 4.1.

The graph shows that the plane wave cutoff converges with the values above 40Ry. Thus in our input preparation 60Ry a value which shows more convergence were used. To test the Convergence of BZ sampling (k-point), we did Convergence of total energy and BZ sampling (k-point), the graph of total energy versus BZ sampling (k-point) is shown in figure 4.2.

The values of K-points converge starting from 5 as the graph shows. Based on this graph we took the values of K-mesh to be 8 8 5 that is a value which can best fit the calculations.

The optimized cell parameters were used in each calculation. In order to investigate the Mn-substitution effects, we have calculated 50% Mn-substitution on Fe site of the parent compound $(NaFe_{0.5}Mn_{0.5}As)$. We did both non-magnetic (NM) and collinear magnetic (Ferromagnetic (FM) and antiferromagnetic (AFM)) ordering calculations using a fixed magnetization = 0.5. This value was used after the convergence test of starting magnetization value. We

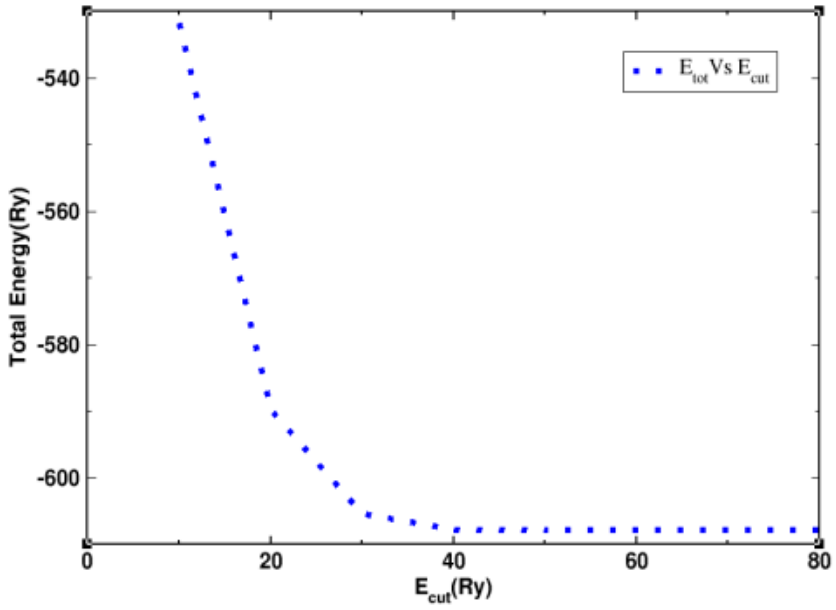

Figure 4.1: Total energy and plane wave cutoff (ecut)

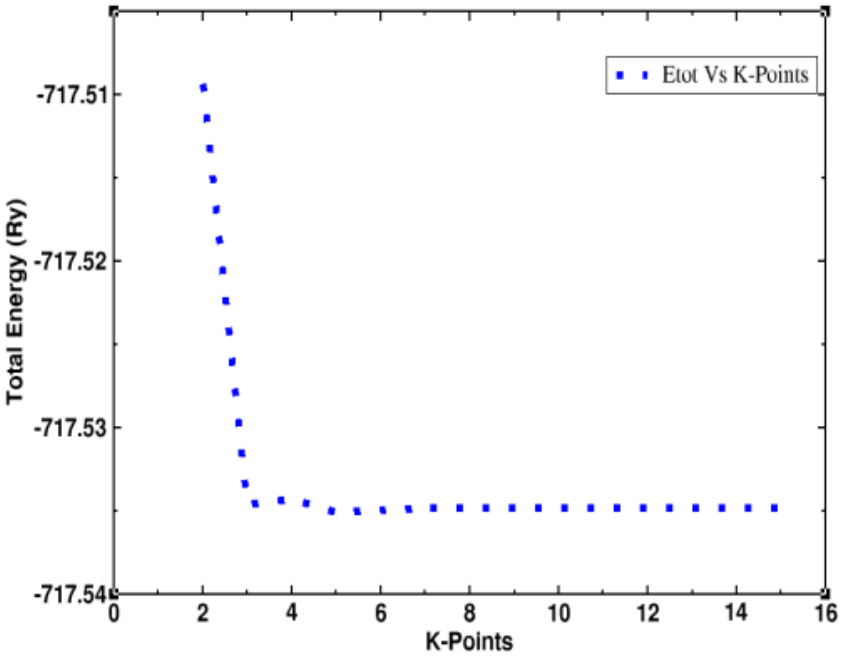

Figure 4.2: Total energy and BZ sampling (k-point)

did this convergency test just like those we did for the BZ and plane wave cutoff. The convergency of magnetization value is done for both the parent compound (NaFeAs) and the 50% Mn substituted Compound ($NaFe_{0.5}Mn_{0.5}As$). The cell parameters we have initially used are $a = b = 3.924[a.u]$ and $c = 6.919[a.u]$. The crystal structures of the parent compound and 50% Mn substituted one are given in figure 4.3 a and b respectively.

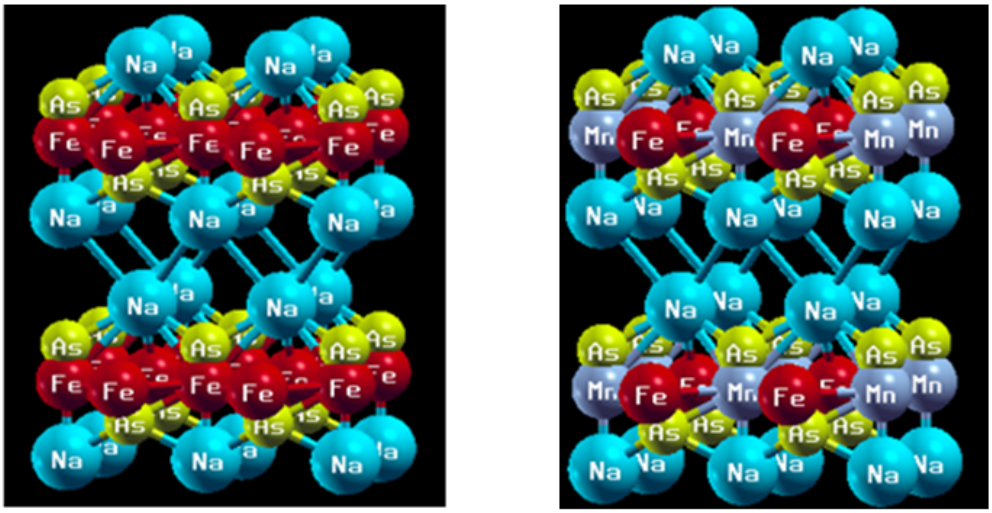

Figure 4.3: The crystal structure of: a) NaFeAs b) $NaFe_{0.5}Mn_{0.5}As$.

The crystal structure of the parent compound is the same as that obtained in Ref 57. The crystal structure of the Mn substituted one is different from the parent compound in that of only two pair of Fe-atoms are observed and the three paired Fe atoms are substituted by the same amount of Mn atoms. The total energies of each compounds (NaFeAs (NM, FM, and AFM) and the 50% Mn substituted ($NaFe_{0.5}Mn_{0.5}As$ (NM, FM, and AFM)) are summarized from the scf calculations and listed in table 4.1.

Table 4.1: The total energies of each compounds after optimization.

Compound	Total Energy (Ry)
NM-NaFeAs	-729.10471712
FM-NaFeAs	-729.10471160
AFM-NaFeAs	-729.10471163
NM-$NaFe_{0.5}Mn_{0.5}As$	-695.07271837
FM-$NaFe_{0.5}Mn_{0.5}As$	-695.06338233
AFM-$NaFe_{0.5}Mn_{0.5}As$	-695.06765503

The table of the total energies indicates that the AFM- ordering shows stability than the FM-ordering. And NaFeAs is more stable than $NaFe_{0.5}Mn_{0.5}As$. That is because the values of total energies of NaFeAs are smaller than those of $NaFe_{0.5}Mn_{0.5}As$ in each calculations. Based on this it can be concluded that NaFeAs is in the ground state than the 50% Mn substituted system. For the convergency of the self-consistent calculations the difference in the total energy of the crystal should not exceed 0.1 mRy as it was mentioned in Ref 14. Thus the difference in the total energy were calculated. In the case of NaFeAs, the energy difference between the energy values of NM and FM is $-5.52\mu Ry$, while that between NM and AFM is $-5.49\mu Ry$. Similarly, in the case of $NaFe_{0.5}Mn_{0.5}As$, the energy difference between NM and FM is $-9.34mRy$, while that between NM and AFM is $-5.06mRy$. Therefore our scf calculation converges.

4.2 Non-Magnetic Ordering Calculations

We did Non-Magnetic (NM) calculations for both the parent compound and 50% Mn substituted. We did the scf, band structure, and DOS calculations after optimization (the optimized lattice parameters were used in these calculations). The electronic band structures we had obtained for NM-NaFeAs and NM-$NaFe_{0.5}Mn_{0.5}As$ along with highly symmetrical points are given in figure 4.4 a and b respectively.

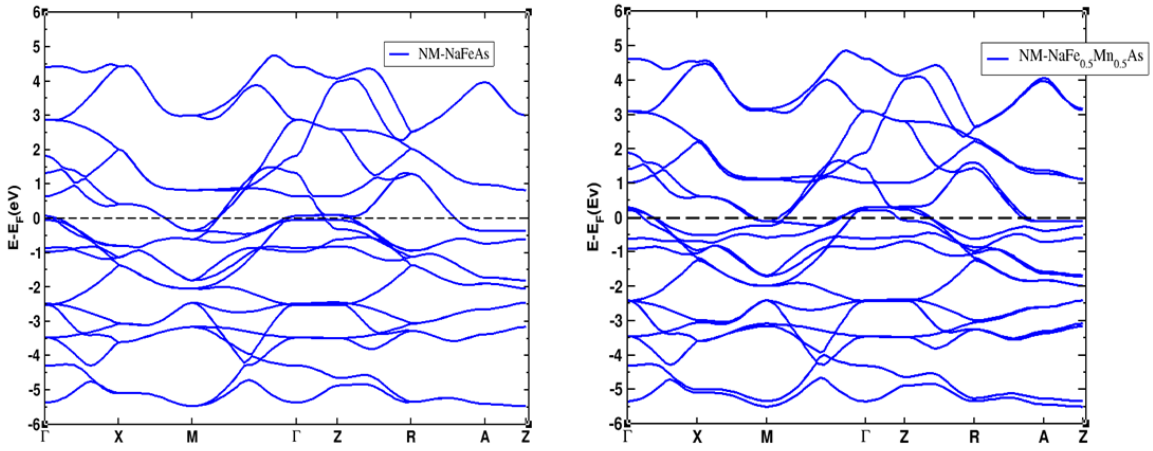

Figure 4.4: Band structures of NM calculations for: a) NaFeAs, b) $NaFe_{0.5}Mn_{0.5}As$.

The band structures of the NM systems (NaFeAs and $NaFe_{0.5}Mn_{0.5}As$) were calculated along the high symmetry points with energy range of -6 eV to 6 eV for both of the parent compound and the 50% Mn substituted one. Our calculated band structure and DOS for NaFeAs are the same to those found in the Ref 60. The NM band structures doesn't show many difference when observed suddenly. But the following points are found as a difference. These are: 1) Many bands cross each other and more approaches to the Fermi-level in between the second Γ and first z-points in the parent compound, indeed in $NaFe_{0.5}Mn_{0.5}As$ there is more gapes between this bands and the Fermi-level the bands being above the Fermi-level, additionally this crossing is not as many as in the parent compound in the 50% Mn substituted. 2)The bands cross the Fermi-level at some points in the parent compound more than which is in the 50% Mn substituted compound this may shows that NaFeAs is highly dense around the Fermi-level than $NaFe_{0.5}Mn_{0.5}As$.

Thus one may conclude that the effect of Mn in the NM-calculation is changing the property of the material by decreasing its density. 3) There is a difference in each band width near the Fermi-level of NaFeAs and $NaFe_{0.5}Mn_{0.5}As$ at each high symmetry points. For instance the band widths near the Fermi-level for the parent compound and the 50% Mn substituted at the first Γ-points are (0.066 eV above the Fermi-level and -0.046 eV below the Fermi-level) for the

parent compound and (0.22 eV above the Fermi-level and -0.6 eV below the Fermi-level) for the Mn substituted, and at the second Γ-points (0.073 eV above the Fermi-level and -0.042 eV below the Fermi-level) for the parent compound and (0.22 eV above the Fermi-level and -0.6 eV below the Fermi-level) for the Mn substituted.

This shows that there is an increment on the band width in the 50% Mn substituted compound. Thus one can conclude that Mn atom increases the band width of the parent compound. The band widths at the rest high symmetry points are given in tables 4.2. 4) The other clearly observed difference is the double degeneracy nature of all bands in between X-M and R-Z points for both systems but this degeneracy in the $NaFe_{0.5}Mn_{0.5}As$ is not as many as in the parent compound. Our calculated DOS in NM-calculations for NaFeAs and $NaFe_{0.5}Mn_{0.5}As$ are given in figure 4.5 a and b respectively.

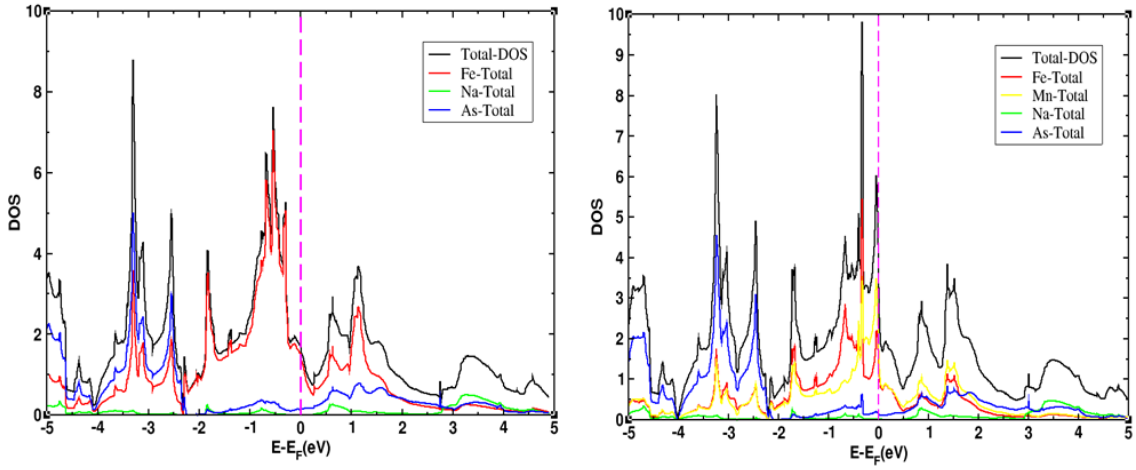

Figure 4.5: DOS of NM calculations for: a) NaFeAs, b) $NaFe_{0.5}Mn_{0.5}As$.

The Calculated projected density of states (DOS) of the parent compound and the 50% Mn substituted systems are within the energy range -5 eV to 5 eV. DOS of each atoms (Fe, As and Na) and total density of states are indicated by red, blue, green, and black lines respectively for the parent compound, and DOS of each atoms (Fe, Mn, As and Na) and total density of states are indicated by red, yellow, blue, green and black lines respectively for the 50% Mn

substituted system. Vertical dotted line at 0 eV represents the Fermi level. The structure of our calculated density of state for the parent compound is the same as which is obtained in Ref 56 and Ref 60. The total density of states at the Fermi-level for the NaFeAs and the 50% Mn substituted are 1.71 states/eV and 3.18 states/eV respectively. This shows that there is an increment of DOS from NaFeAs to $NaFe_{0.5}Mn_{0.5}As$ at the Fermi-level.

Although the total DOS of $NaFe_{0.5}Mn_{0.5}As$ at Fermi-level is greater than that of the parent compound DOS, it rapidly drops near the Fermi-level in the conduction band. So, we can conclude that Mn atom changes the nature of the DOS of NaFeAs near the Fermi-level. In both cases the density of state shows that both compounds are denser below the Fermi-level. But above the Fermi-level the parent compound is denser than the 50% Mn substituted one. The other difference is on the nature of the DOS near the Fermi-level, that is it shows a little peak in the valance band and then slowly decreases near the Fermi-level in the conduction band for the parent compound, but for the 50% Mn substituted compound it increases in the valance band and rapidly drop in the conduction band then moving a lot it shows a very small peak then it decreases again.

While we compare the role of each atoms, It is clear from the projected DOS curves that within the energy range of E_F =2eV, the electronic states are of predominant Fe-atom which determines the physical properties of the system, thus Fe-atom dominates all of the others having a maximum peak of 7.037 states/eV below the Fermi-level, 2.7 states/eV above the Fermi-level and 1.51 states/eV at the Fermi-level in the parent compound and, 5.43 states/eV below the Fermi-level, 1.12 states/eV above the Fermi-level and 1.3 states/eV at the Fermi-level in the 50% Mn substituted. Next to the Fe-atom As-atom shows a little peak near the Fermi-level in both compounds and Na-atom shows very small DOS in both conduction and valance bands and it is almost diminished near and at the Fermi-level in both systems. Finally the Mn-atom shows dominance next to the Fe-atom above the Fermi-level but the DOS of this atom is greater than that of the Fe-atom at the Fermi-level with a value of 1.61 states/eV. Thus Mn atom shows dominance in $NaFe_{0.5}Mn_{0.5}As$.

Thus in the parent compound, the small projected DOS of Na in the energy range of interest leads to a much weaker Na-As bonding if compared to Fe-As and Fe-Fe. These properties are the same to the idea expressed in the Ref 60 "The strong Fe-As covalency determines the bonding in the two dimensional Fe-As layer, while the partial ionic bonding between Na-As determines the packing of these layers".

4.3 Ferromagnetic Ordering Calculation

We did Ferromagnetic (FM) ordering calculations for both the parent compound and 50% Mn substituted system. We also did the scf, band structure, and DOS calculations after optimization. Our calculated electronic band structures for FM NaFeAs and $NaFe_{0.5}Mn_{0.5}As$ along with highly symmetrical points are given in figure 4.6 a and b respectively.

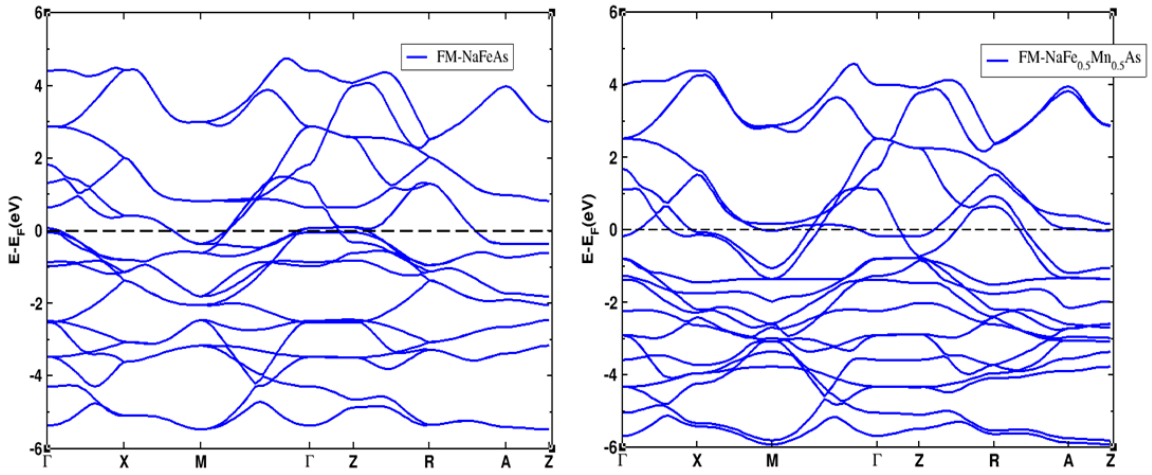

Figure 4.6: Band structures of FM calculations for: a) NaFeAs, b) $NaFe_{0.5}Mn_{0.5}As$.

For the FM systems (NaFeAs and $NaFe_{0.5}Mn_{0.5}As$) the band structures are calculated along the high symmetry points with energy range of -6 eV to 6 eV for both of the parent and the 50% Mn substituted compounds. Here we have observed the following difference. These are 1) In the parent compound many bands cross each other and some flat bands those cross each

other are more approach to the Fermi-level between the second Γ and first z-points. Indeed this crossing is infrequent rather the bands are sparse (thin) in the 50% Mn substituted compound and this bands lies below the Fermi-level. This implies that the substitution of Mn in this system suppress the density of the parent compound. 2) The bands cross the Fermi-level at some points, and many of them are flat in the parent compound more than which is in the 50% Mn substituted compound.

Additionally, the double degeneracy nature of all bands in between X-M and R-Z points in the $NaFe_{0.5}Mn_{0.5}As$ is very small in this ordering. 3) There are also some differences in each band width near the Fermi-level of NaFeAs and $NaFe_{0.5}Mn_{0.5}As$ at the high symmetry points. For instance the band widths near the Fermi-level for the parent compound and the 50% Mn substituted at the first Γ-points are (0.076 eV above the Fermi-level and -0.047 eV below the Fermi-level) for the parent compound and (1.12 eV above the Fermi-level and -0.18 eV below the Fermi-level) for the Mn substituted, and at the second Γ-points (0.076 eV above the Fermi-level and -0.048 eV below the Fermi-level) for the parent compound and (1.11 eV above the Fermi-level and -0.16 eV below the Fermi-level) for the Mn substituted. This shows that there is an increment on the band width in the 50% Mn substituted compound. Thus one can conclude that Mn atom increases the band width of the parent compound. The band widths at the rest points are given in table 4.2. Our calculated DOS in FM-ordering calculations obtained for NaFeAs and $NaFe_{0.5}Mn_{0.5}As$ are given in figure 4.7 a and b respectively.

The Calculated projected DOS of the normal compound and the 50% Mn substituted systems are with the energy range of -5 eV to 5 eV. DOS of each atoms (Fe, As and Na) and total density of states are indicated by red, blue, green, and black lines respectively for the parent compound, and DOS of each atoms (Fe, Mn, As and Na) and total density of states are indicated by red, yellow, blue, green and black lines respectively for the 50% Mn substituted system. Vertical dotted line at 0 eV represents the Fermi level. The total density of state at the Fermi-level for the NaFeAs and the 50% Mn substituted are 1.7states/eV and 1.98 states/eV respectively. This shows that there is an increment of DOS from NaFeAs to $NaFe_{0.5}Mn_{0.5}As$.

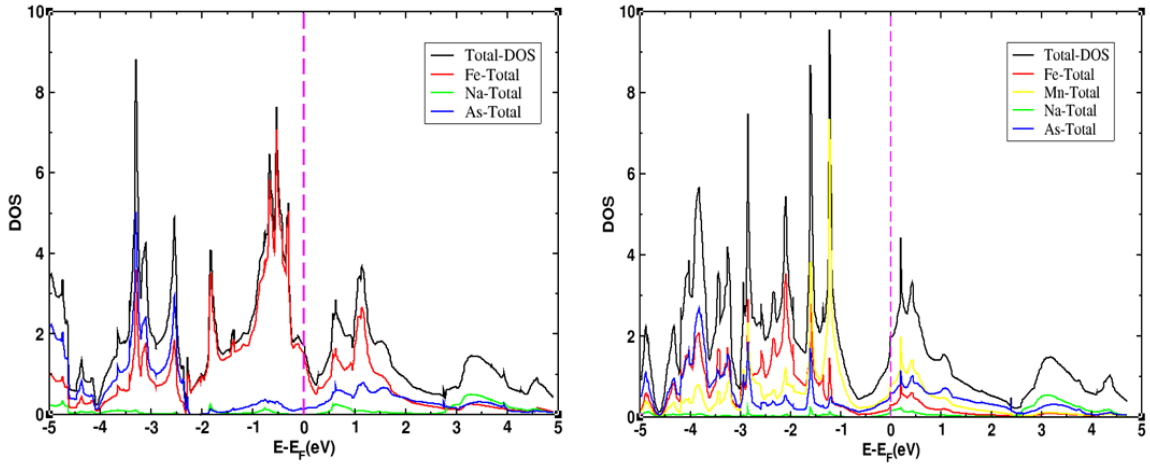

Figure 4.7: DOS of FM calculations for: a) NaFeAs, b) $NaFe_{0.5}Mn_{0.5}As$.

Based on this difference one can conclude that the substitution of Mn atom enhance the DOS of NaFeAs. The other un expected difference is the high contribution of the As-atom in the $NaFe_{0.5}Mn_{0.5}As$. In spite of the fact that As-atom plays very small role in the parent compound, it dominates Fe and Na-atoms at and near the Fermi-level in the energy range from -1 eV to 2.5 eV in the 50% Mn substituted system.

In both cases the density of state shows that both compounds are dense below the Fermi-level. But above the Fermi-level the 50% Mn substituted system is denser than the parent compound. That might be due to the maximum peak in the DOS of Mn-atom above the Fermi-level in this system. Concerning to the nature of the DOS near the Fermi-level, the DOS of the parent compound shows the same property with the one shown in the NM-calculation. But in the 50% Mn substituted compound the DOS shows some difference from that obtained in the NM-calculation. That is slightly increasing in the valance band then it highly increases in the conduction band. While we compare the role of each atoms, the Fe-atom dominates all of the others having a maximum peak of 7.05 states/eV below the Fermi-level, 2.65 states/eV above the Fermi-level and 1.53 states/eV at the Fermi-level in the parent compound and, 3.53 states/eV below the Fermi-level, 0.87 states/eV above the Fermi-level and 0.3 states/eV at the Fermi-level in the 50% Mn substituted.

Next to the Fe-atom As-atom shows small peak in the parent compound and Na-atom shows very small DOS in both conduction and valance bands and it is almost diminished near and at the Fermi-level in NaFeAs But in the 50% Mn substituted case the Fe-atom is dominated by As-atom near and at the Fermi-level as it was mentioned above. Finally the Mn-atom shows dominance in the energy range around -2.5 eV to 2.5 eV. The DOS of this atom is also greater than that of the Fe atom at the Fermi-level with a value of 0.83 states/eV. Thus Mn atom shows dominance in $NaFe_{0.5}Mn_{0.5}As$.

4.4 Antiferromagnetic Ordering Calculation

Finally we did antiferromagnetic (AFM) calculations for both the parent compound and 50% Mn substituted. As usual we did the scf, band structure, and DOS calculations after optimization. Our calculated electronic band structures for AFM NaFeAs and $NaFe_{0.5}Mn_{0.5}As$ along with highly symmetrical points are given in figure 4.8 a and b respectively.

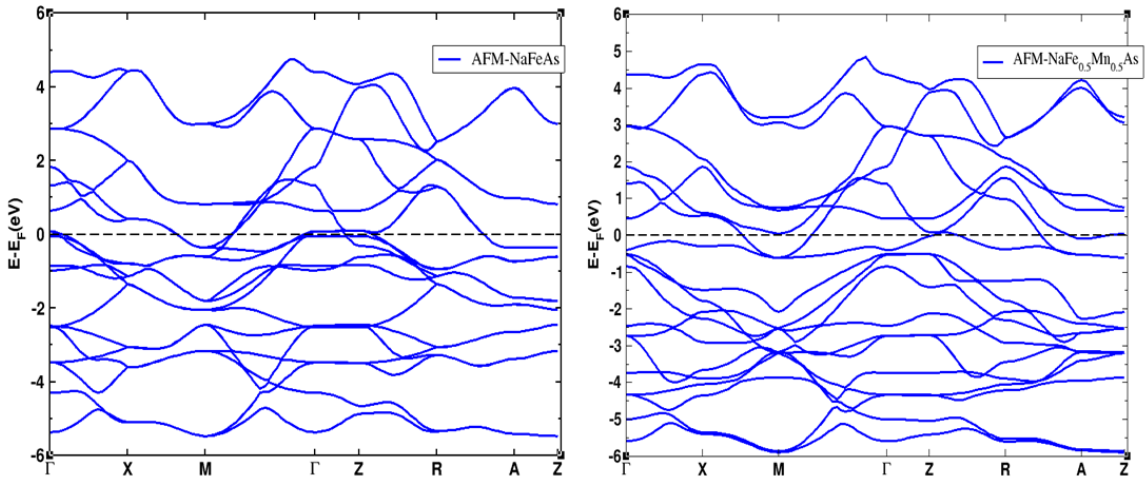

Figure 4.8: Band structures of AFM calculations for: a) NaFeAs, b) $NaFe_{0.5}Mn_{0.5}As$.

For the AFM systems (NaFeAs and $NaFe_{0.5}Mn_{0.5}As$) the band structures are calculated along the high symmetry points with energy range of -6 eV to 6 eV for both of the parent and the 50%

Mn substituted compounds. In the AFM band structures we have observed the following difference. 1) In the parent compound many bands cross each other between the second Γ and first Z-points at the Fermi-level and this bands overlapped on each other being very approach to the Fermi-level in addition to this, they are flat bands, but there is a decrement of such crossing and flat bands rather some bands are curved in the 50% Mn substituted compound. This shows that the Mn atom changes the nature of the bands. 2) The bands cross the Fermi-level at many points in NaFeAs more than which is in the 50% Mn substituted compound and there is a difference in each band width near the Fermi-level of NaFeAs and $NaFe_{0.5}Mn_{0.5}As$ at the high symmetry points.

For instance the band widths near the Fermi-level for the parent compound and the 50% Mn substituted at the first Γ-points are (0.072 eV above the Fermi-level and -0.045 eV below the Fermi-level) for the parent compound and (0.452 eV above the Fermi-level and -0.41 eV below the Fermi-level) for the Mn substituted, and at the second Γ-points (0.072 eV above the Fermi-level and -0.04 eV below the Fermi-level) for the parent compound and (0.45 eV above the Fermi-level and -0.4 eV below the Fermi-level) for the Mn substituted system. This shows that there is an increment on the band width in the 50% Mn substituted compound. Thus one can conclude that Mn atom increases the band width of the parent compound. The band widths at the rest points are given in table 4.2. 3) In addition to the narrowness of the band width at the first Γ-points near the Fermi-level, these bands are many at this point. That is at this point the bands are denser in the parent compound but in the 50% Mn substituted compound the bands are very sparse and far away from the Fermi-level in this calculation.

Thus the presence of Mn-atom changes the property of the band structure in the AFM calculation more than which is in FM and NM calculations. 4) The other difference which is not observed in the NM and FM-calculations is that the bands above the Fermi-level overlap on each other (there is double degeneracy nature) in the parent compound but in the Mn substituted compound these bands are very sparse (thin) (there is no any double degeneracy nature). Likewise the double degeneracy nature along X-M and R-A points is completely

absent in the case of $NaFe_{0.5}Mn_{0.5}As$ in this ordering. The calculated density of states in AFM-calculations obtained for NaFeAs and $NaFe_{0.5}Mn_{0.5}As$ are given in figure 4.9 a and b respectively.

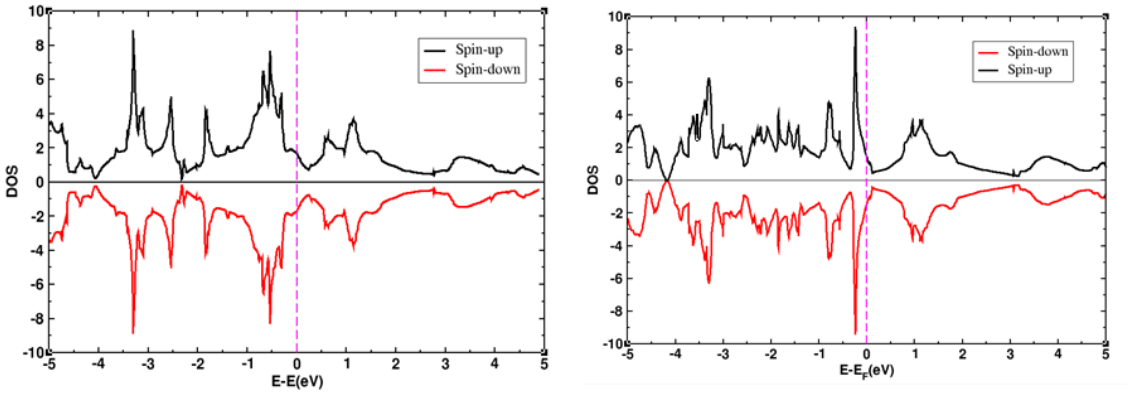

Figure 4.9: DOS of AFM calculations for: a) NaFeAs, b) $NaFe_{0.5}Mn_{0.5}As$.

The Calculated DOS of the parent compound and the 50% Mn substituted systems are within the energy range -5eV to 5eV. DOS of the spin-up electrons is represented by the black line in the positive y-axis whereas that of the spin-down is represented by red line in the negative y-axis. Vertical dotted line at 0eV represents the Fermi-level.

The nature of the DOS near the Fermi-level decreases slightly from the valance band to the conduction band then after it shows a slight increment for the parent compound, but for the 50% Mn substituted compound it decreases rapidly in the valance band and increases slightly in the conduction band. The density of state at the Fermi-level for NaFeAs and the 50% Mn substituted system are (1.71 states/eV for the spin-up and -1.71 states/eV for the spin-down) and (1.4 states/eV for the spin-up and -1.4 states/eV for the spin-down) respectively. This shows that there is decrement of DOS from NaFeAs to $NaFe_{0.5}Mn_{0.5}As$ (the DOS at the Fermi-level drop due to the substitution of Mn atom). Based on this difference one can conclude that Mn-atom suppress the DOS of the parent compound. In both cases the density of state shows that both compounds are dense below the Fermi-level.

Table 4.2: The band widths in unit of electro Volt (eV) near the Fermi-level at each high symmetry points. F-L is the Fermi-level.

High Symmetry Points	NaFeAs			$NaFe_{0.5}Mn_{0.5}As$		
	NM	FM	AFM	NM	FM	AFM
Γ above F-L	0.066	0.076	0.072	0.22	1.12	0.45
Γ below F-L	-0.046	-0.047	-0.45	-0.6	-0.18	-0.41
X above F-L	0.42	0.42	0.42	0.63	1.51	0.54
X below F-L	-0.79	-0.79	-0.79	-0.5	0.075	-0.3
M above F-L	0.83	0.82	0.83	1.11	0.17	0.042
M below F-L	-0.36	-0.35	-0.35	-0.094	-0.037	-0.6
Γ above F-L	0.073	0.076	0.072	0.22	1.11	0.45
Γ below F-L	-0.042	-0.048	-0.04	-0.6	-0.16	-0.39
Z above F-L	0.095	0.099	0.1	0.25	2.25	0.09
Z below F-L	-0.042	-0.046	-0.045	-0.086	-0.17	-0.041
R above F-L	1.3	1.3	1.3	1.43	0.64	0.98
R below F-L	-0.94	-0.94	-0.94	-1.61	-1.5	-0.37
A above F-L	0.99	0.987	0.99	1.28	0.03	0.7
A below F-L	-0.35	-0.34	-0.36	-0.1	-1.2	-0.1
Z above F-L	0.82	0.84	0.83	1.13	0.17	0.042
Z below F-L	-0.352	-0.35	-0.36	-0.1	-0.02	-0.6

4.5 Critical Temperature Calculation and magnetic properties

The superconducting transition temperature is calculated as a function of the electron-phonon coupling constant. Using the MacMillan's Formula as mentioned in equation 2.2. We have calculated the values of the critical temperature for each compound in NM, FM and AFM ordering calculations. We did the calculation by using the electron-phonon coupling constant λ = 0.8 and the Debye characteristic phonon frequency Θ =215 K from Ref 60. Then we obtain T_C =9.33 K in the parent compound T_C = 8.4 K in the 50% Mn substituted compound for the NM calculation. Here the critical temperature of NaFeAs drops when Mn-atom is substituted in it. Thus Mn-atom suppresses the T_C of this compound. Like wise in the FM-ordering calculation the T_C value of NaFeAs decreases due to the substituted Mn-atom having values of T_C = 9.36 K and 9.1K for the parent and 50% Mn substituted compounds respectively. The calculated value of T_C increases in the AFM-ordering calculation having values of (9.33 K in the parent compound and 9.7 K in the 50% Mn substituted compound). The suppression of T_C due to Mn substitution in the NM ordering leads this compound to adopt the property of the rest IBSCs. Our calculated value of T_C for the parent compound approaches to the value obtained in Ref 57.

To understand the magnetic properties of these compounds, the total magnetization and the magnetic moment of all systems are observed. In the FM-ordering calculation the total magnetization of the parent compound is -0.01 Bohr magneton/cell and 3.64 Bohr magneton/cell in the 50% Mn substituted system. In the case of AFM-ordering calculation the total magnetization is 0 and -0.44 Bohr magneton/cell for the parent compound and the 50% Mn substituted one respectively. Here the total magnetization of the FM-ordering shows enhancement and that of the AFM-ordering is found to decrease. Thus one can conclude that the substitution of Mn atom might be responsible for these variation in magnetization.

The magnetic moment of each systems under FM and AFM-ordering calculations are tabulated in table 4.3. To understand the magnetic properties of the 50% Mn substituted system,

the Fe and Mn magnetic moments were computed. The calculated magnetic moment of the Fe-atom for the FM-NaFeAs is in approximate withe the value obtained in Ref 14. According to the results summarized in this table, the Fe magnetic moment shows enhancement in the 50% Mn substituted system when compered with that of the parent compound. Based on this we can conclude that this enhancement is due to the substituted Mn-atom.

Table 4.3: The calculated magnetic moment values of Fe and Mn-atoms in Bohr magneton/cell.

Compound	Fe-Magnetic Moment	Mn-Magnetic Moment
FM-NaFeAs	0.0017	
AFM-NaFeAs	0.0041	
FM-$NaFe_{0.5}Mn_{0.5}As$	1.56	2.03
AFM-$NaFe_{0.5}Mn_{0.5}As$	2.06	2.39

5. Conclusions and Recommendations

In this paper we have investigated the effect of Mn substitution at the Fe site in NaFeAs. In order to investigate this effects, we did 50% Mn-substitution on Fe site of the parent compound ($NaFe_{0.5}Mn_{0.5}As$). DFT calculations as implemented in quantum ESPRESSO were used to calculate the electronic structures of NaFeAs and $NaFe_{0.5}Mn_{0.5}As$. The basic self-consistent field calculation (scf), Convergence of the plane waves cutoff (ecut), Convergence of the BZ sampling (k-point), Lattice constant (vc-relax Calculation) which is optimization of cell parameters were done. Using the optimized cell parameters each calculations(the scf, band and DOS) were done. The crystal structure of the parent compound is obtained and it is the same as the one given in Ref 57 and that of the 50% Mn-substituted system is also obtained.

The band structure and the DOS are calculated for both systems. The calculation was done for non-magnetic (NM) and collinear-magnetic (AFM and FM) behaviors. Comparison was done between the two systems (NaFeAs and $NaFe_{0.5}Mn_{0.5}As$) that are NM- NaFeAs with NM-$NaFe_{0.5}Mn_{0.5}As$, and likewise the AFM and FM behaviors are compered. The band structure in the NM and FM- calculations shows less difference where in the AFM-calculation the two bands are completely different at the first Γ-point and in between the second Γ-point and the first Z-point. The double degeneracy nature of all bands in between X-M and R-A points are observed in the parent compound in each orderings, but it decreases in the FM- ordering and Completely disappear in the AFM-ordering.

In NaFeAs, the plots of the DOS show some generic features that are common to the parent compounds of the iron-based superconductors. The DOS is dominated by the Fe states around the Fermi-level, having a small contribution from the As and Na states and that is strongly decreasing with energy near the Fermi-level. Our calculated value of T_c =9.33 K of NaFeAs more approaches to the result obtained in Ref 57. Concerning to the DOS in the AFM behavior NaFeAs has high DOS value than the FM. This may shows that a strong electron-phonon interaction via hybridization of appropriate electron states near, the Fermi level exist in the AFM system. The substitution of Mn atom also cause variation in magnetic moment. The increment of the DOS near the Fermi-level in NM and FM-calculations contradicts to the previous studies regarding to IBSC. Thus further study is necessary on this area. It is already known that the Fe based compounds have robustness properties to impurity addition. Thus it is necessary to concentrate on finding Fe based HTS using impurities, because HTS can be used for many advantages for instance they can be used for electric power grid without any energy lost.

Research Fund Acknowledgment

This research project is funded by Adama Science and Technology University under the grant number $ASTU/SM-R/257/21$, Adama, Ethiopia.

Bibliography

[1] Kittel, C. (2021). Introduction to solid state physics, Eighth edition.

[2] Hirsch, J. E. (2016). On the dynamics of the Meissner effect. *Physica Scripta*, 91, 035801.

[3] Oh, H., Moon, J, Shin, D., Moon, C. Y., and Choi, H. J. (2011). Brief review on iron-based superconductors: are there clues for unconventional SC, 89, 2011.

[4] Baldent, V., Rullier-Albenque, F., Colson, D., Ablett, J. M., and Rueff, J. P.(2015). Electronic properties of $BaFe_2As_2$ upon doping and pressure: the prominent role of the As p orbitals. *Physical review letters*, 114, 177001.

[5] Hosono, H., and Kuroki, K. (2015). Iron-based superconductors: Current status of materials and pairing mechanism. *Physica C: Superconductivity and its Applications,* 514, 399-422.

[6] Liang, W., Chen, J., Liu, Y., and Chen, S. (2014). Density-functional-theory calculation analysis of active sites for four-electron reduction of O_2 on Fe/N doped graphene. *Acs Catalysis*, 4, 4170-4177.

[7] Becke, A. D. (2014). Perspective: Fifty years of density-functional theory in chemical physics. T*he Journal of chemical physics*,140, 18A301.

[8] Isaacs, E. B., and Wolverton, C. (2018). Inverse band structure design via materials database screening: application to square planar thermo electrics. *Chemistry of Materials*, 30, 1540-1546.

[9] Shiri, H. M., Ehsani, A., Behjatmanesh-Ardakani, R., and Hajghani, S. (2019). Electro synthesis of Y_2O_3 nanoparticles and its nano composite with POAP as high efficient electrode materials in energy storage device: Surface, 53 54 density of state and electrochemical investigation. *Solid State Ionics*, 338, 87- 95

[10] Chowdhury, U. K., and Islam, M. R. (2018). The Properties, Advantage, Disadvantage and Applications of Iron-Based Superconductors: AReview Work. *International Journal of Advanced Research in Physical Science*, 5, 16-31.

[11] Chu, C. W., Chen, F., Gooch, M., Guloy, A. M., Lorenz, B., Lv, B. and Xue, Y. Y. (2009). The synthesis and characterization of LiFeAs and NaFeAs. *Physica C: Superconductivity*, 469, 326-331.

[12] Hammerath, F., Bonf, P., Sanna, S., Prando, G., De Renzi, R., Kobayashi, Y and Carretta, P. (2014). Poisoning effect of Mn in $LaFe_{1-x}Mn_xAsO_{0.89}F_{0.11}$:: Unveiling a quantum critical point in the phase diagram of iron-based superconductors. *Physical Review B*, 89, 134503.

[13] Song, Y., Wang, W., Paris, E., Lu, X., Pelliciari, J., Tseng, Y, and Dai, P. (2021). Spin dynamics in NaFeAs and $NaFe_{0.53}Cu_{0.47}As$ probed byresonant inelastic x-ray scattering. *Physical Review B*, 103, 075112.

[14] Mahesh, R., and Reddy, P. V. (2019). Electronic, Structural, and Magnetic Properties of Hole-Doped Iron-Based Superconductors Using First Principle Study. *Journal of Superconductivity and Novel Magnetism*, 1-10.

[15] Amit Roy. (2017). Story of superconductivity, *Resonance*, Vol. 22, pp. 461-473.

[16] Hongisto, T., and Arutyunov, K. Y. (2008, February). Persistent currents in superconducting nanorings. *In Journal of Physics*, 97, 1, 012114.

[17] Paglione, J., and Greene, R. L. (2010). High-temperature superconductivity in iron-based materials. *Nature physics*, 6, 645-658.

[18] Dou, S. X., Braccini, V., Soltanian, S., Klie, R., Zhu, Y., Li, S. and Larbalestier, D. (2004). Nanoscale-SiC doping for enhancing j_c and H_{C2} in superconducting MgB_2. Journal of Applied physics, 96, 7549-7555.

[19] Sharma, R. G. (2021). Superconductivity: *Basics and applications to magnets* ,214.

[20] Pal, S. (2020). BCS theory of superconductivity: a pedagogic short review by mathematical descriptions. *International Journal of Innovative Research in Physics*, 1, 15-37.

[21] Boovic, I., Bollinger, A. T., Wu, J., and He, X. (2018). Can high-Tc superconductivity in cuprates be explained by the conventional BCS theory? *Low Temperature Physics*, 44(6), 519-527.

[22] Torrens, F., and Castellano, G. (2018). Superconductors, superconductivity, BCS theory, and entangled photons for quantum computing. *In Physical Chemistry for Engineering and Applied Sciences*, 401-410.

[23] Sirohi, A., Das, S., Adhikary, P., Chowdhury, R. R., Vashist, A., Singh, Y, and Sheet, G. (2019). Mixed type I and type II superconductivity due to intrinsic electronic in homogeneities in the type II Dirac semimetal $PdTe_2$. *Journal of Physics: Condensed Matter*, 31, 085701.

[24] Karci, . (2015). Design of a Self-Aligned, High Resolution, Low Temperature (30 Mk-300 K) *Magnetic Force Microscope* , 134, 20151.

[25] GR Stewart. (2017). " Unconventional superconductivity," *Advances in Physics*, 66, 75196.

[26] De Simoni, G., Paolucci, F., Solinas, P., Strambini, E., and Giazotto, F. (2018). Metallic supercurrent field-effect transistor. *Nature nanotechnology*, 13, 802- 805.

[27] Abdel-Hafiez, M., Ge, J., Vasiliev, A. N., Chareev, D. A., Van de Vondel, J., Moshchalkov, V. V., and Silhanek, A. V. (2013) Temperature dependence of 55 56 lower critical field $H_{C1}(T)$ shows node less superconductivity in FeSe. *Physical Review B*, 88, 174512.

[28] Hirvonen, L. M., and Suhling, K. (2020). Fast timing techniques in FLIM applications. *Frontiers in Physics*, 8, 161.

[29] Boeri, L., Dolgov, O. V., and Golubov, A. A. (2008). Is $LaFeAsO_{1-x}F_x$ an electron-phonon superconductor? *Physical Review Letters*, 101, 026403.

[30] Van Delft, D. (2012). History and significance of the discovery of superconductivityby Kamerlingh Onnes in 1911. *Physica C: Superconductivity*,479, 30-35.

[31] Hosono, H., Yamamoto, A., Hiramatsu, H., and Ma, Y. (2018). Recent advances in iron-based superconductors toward applications. *Materials today*, 21(3), 278-302.

[32] Fujitsu, S., Matsuishi, S., and Hosono, H. (2012). Iron based superconductors processing and properties. *International materials reviews*, 57(6), 311-327

[33] Dahal, K. P. (2011). Superconductivity: A Centenary Celebration. *Himalayan Physics*, 2, 26-34

[34] Cao, G. H., Jiao, W. H., Luo, Y. K., Ren, Z., Jiang, S., and Xu, Z. A. (2012, December). Co-existence of superconductivity and ferromagnetism in iron pnictides. *In Journal of Physics: Conference Series* (Vol. 391, No. 1, p. 012123). IOP Publishing.

[35] Kamihara, Y., Watanabe, T., Hirano, M., and Hosono, H. (2008). Iron-based layered superconductor $La[O_{1-x}F_x]FeAs(x = 0.05 - 0.12)$ with $T_c = 26K$. *Journal of the American Chemical Society*, 130, 3296-3297.

[36] Pallecchi, I., Tarantini, C., Hnisch, J., and Yamamoto, A. (2020). Preface to the special issue focus on 10 years of iron-based superconductors, *SST*, Vol. 33.

[37] Craco, L., Laad, M. S., and Leoni, S. (2014). Orbital-selective mottness in layered iron oxychalcogenides: the case of $Na_2Fe_2OSe_2$, *Journal of Physics: Condensed Matter*, Vol. 26, no. 145602.

[38] Li, W. M., Zhao, J. F., Cao, L. P., Hu, Z., Huang, Q. Z., Wang, X. C., ... and Jin, C. Q. (2019). Superconductivity in a unique type of copper oxide. *Proceedings of the National Academy of Sciences*, 116, 12156-12160.

[39] Chen, X., Dai, P., Feng, D., Xiang, T., and Zhang, F. C. (2014). Iron-based high transition temperature superconductors. *National Science Review*, 1, 371- 395.

[40] Liu, S. L., and Zhou, T. (2012). Effect of transition-metal substitution in iron based superconductors. *Journal of Physics: Condensed Matter*, 24, 225701.

[41] Miyasaka, S., Suzuki, S., and Tajima, S. (2016). Superconducting Gap Symmetry of LaFeP (O, F) Observed by Impurity Doping Effect. *Symmetry*, 8, 80.

[42] Oh, H., Moon, J., Shin, D., Moon, C. Y., and Choi, H. J. (2011). Brief review on iron-based superconductors: are there clues for unconventional superconductivity, 1201, 0237.

[43] Thakur, G. S., Haque, Z., Neha, P., Gupta, L. C., Patnaik, S., and Ganguli, A. K. (2014). Effect of O-and Mn-Doping on Superconductivity in $FeTe_{0.5}Se_{0.5}$ Superconductor. *Zeitschrift fr anorganische und allgemeine Chemie*, 640, 1159-1163.

[44] Thaler, A. (2012). " Structural and magnetic properties and superconductivity in $Ba(Fe_{1-x}Tmx)_2As_2(Tm = Ru, Mn, Cr/Co, Mn/Co)$ *single crystals*," vol. 2.

[45] Rosa, P. F. S., Adriano, C., Garitezi, T. M., Piva, M. M., Mydeen, K., Grant, T, and Pagliuso, P. G. (2014). Possible unconventional superconductivity in substituted $BaFe_2As_2$ revealed by magnetic pair-breaking studies. *Scientific reports*, 4, 1-6.

[46] Deng, Q., Ding, X., Li, S., Tao, J., Yang, H., and Wen, H. H. (2014). "The effect of impurity and the suppression of superconductivity in $Na(Fe_{0.97-x}Co_{0.03}Tx)As(T = Cu, Mn)$," *New Journal of Physics*, 16, 063020.

[47] Steckel, F., Beck, R., Roslova, M., Abdel-Hafiez, M., Wolter, A. U., Morozov, I, and Bchner, B. (2015). "Characterization of doped $Na(Fe_{1-x}T_x)$ single crystals withT= Pd,Ni, Cr, and Mn," *Journal of Superconductivity and Novel Magnetism* , 28, 11231127.

[48] Liu, Y., Bao, J. K., Zuo, H. K., Ablimit, A., Tang, Z. T., Feng, C. M., and Cao, G. H. (2016). " Effect of impurity scattering on superconductivity in $K_2Cr_3As_3$," 59, 657402.

[49] Andersen, L., Ramires, A., Wang, Z., Lorenz, T., and Ando, Y. (2020). Generalized Anderson? theorem for superconductors derived from topological insulators. *Science advances*, 6, 6502.

[50] de La Cruz, Clarina, Q. Huang, J. W. Lynn, Jiying Li, W. Ratcliff Ii, Jerel L. Zarestky, H. A. Mook (2008). " Magnetic order close tosuperconductivity in the iron-based layered $LaO_{1-x}F_xFeAs$ systems," *nature*,453 , 899-902.

[51] Biswal, G., and Mohanta, K. L. (2021). A recent review on iron-based superconductor. *Materials Today: Proceedings*, 35, 207-215.

[52] Doiron-Leyraud, N., Proust, C., LeBoeuf, D., Levallois, J., Bonnemaison, J. B., Liang, R., and Taillefer, L. (2007). Quantum oscillations and the Fermi surface in an under doped high-T c superconductor.*Nature*, 447, 565-568.

[53] Murphy, J., Tanatar, M. A., Kim, H., Kwok, W., Welp, U., Graf, D, and Prozorov, R. (2013). "Effect of heavy-ionirradiation on londonpenetration depth in overdoped $(Fe_{1-x}Co_x)_2As_2$,"*Physical Review* , 88, 054514.

[54] Yi, M., Lu, D. H., Moore, R. G., Kihou, K., Lee, C. H., Iyo, A., and Shen, Z. X. (2012). Electronic reconstruction through the structural and magnetic 59 transitions in detwinned NaFeAs. *New Journal of Physics*, 14, 073019.

[55] He, C., Zhang, Y., Xie, B. P., Wang, X. F., Yang, L. X., Zhou, B., ... and Feng, D. L. (2010). Electronic-structure-driven magnetic and structure transitions in superconducting NaFeAs single crystals measured by angle-resolved photoemission spectroscopy. *Physical review letters*, 105(11), 117002.

[56] Jishi, R. A., and Alyahyaei, H. M. (2010). Electronic and lattice dynamical properties of the iron-based superconductors LiFeAs and NaFeAs. *Advances in condensed matter physics*, 2010.

[57] Parker, D. R., Pitcher, M. J., Baker, P. J., Franke, I., Lancaster, T., Blundell, S. J., and Clarke, S. J. (2009). Structure, ant ferromagnetism and superconductivity of the layered iron arsenide NaFeAs. *Chemical Communications*, (16), 2189-2191.

[58] J.H. Tapp, Z. Tang, Bing. Lv, K. Sasmal, B. Lorenz, Pcwchu, and Amguloy (2008). *Phys. Rev*, 78, 60505.

[59] Michael J. Pitcher, Dinah R. Parker, Paul Adamson, Sebastian J. C. Herkelrath, Andrew T. Boothroyd and Simon J. Clarke(2008). "Structure andsuperconductivity of LiFeAs. *Chemical Communications*," 45,59185920.

[60] Deng, S., Khler, J., and Simon, A. (2009). Electronic structure and lattice dynamics of NaFeAs. Physical Review B, 80, 214508.

[61] Chowdhury, U. K., and Islam, M. R. (2018). The Properties, Advantage, Disadvantage and Applications of Iron-Based Superconductors: A Review Work. *International Journal of Advanced Research in Physical Science*, 5, 16-31

[62] Villar Arribi, P., and de'Medici, L. (2021). Hund's metal crossover and superconductivity in the 111 family of iron-based superconductors, 2104.

[63] Parker, D. R., Smith, M. J., Lancaster, T., Steele, A. J., Franke, I., Baker, P. J,and Clarke, S. J. (2010). Control of the competition between a magnetic phase and a superconducting phase in cobalt-doped and nickel-doped NaFeAs using electron count. *Physical review letters*, 104, 057007.

[64] Wang, X. C., Liu, Q. Q., Deng, Z., Lv, Y. X., Gao, W. B., Zhang, S. J., and Jin, C. Q. (2010). The Study of the Properties for 111 Type Iron Arsenide Superconductor. *Journal of superconductivity andnovel magnetism*, 23, 583

[65] Song, Y., Wang, W., Paris, E., Lu, X., Pelliciari, J., Tseng, Y, and Dai, P. (2021). "Spin dynamics in NaFeAs and $NaFe_{0.53}Cu_{0.47}As$ probed by resonant inelastic x-ray scattering," *Physical Review*, 103 ,075112,.

[66] Ye, Z. R., Zhang, Y., Chen, F., Xu, M., Jiang, J., Niu, X. H, and Feng, D. L. (2014). Extraordinary doping effects on quasiparticle scattering and bandwidth in iron-based superconductors. *Physical Review* X,4, 031041.

[67] Ma, L., Chen, G. F., Yao, D. X., Zhang, J., Zhang, S., Xia, T. L., and Yu, W. (2011). Na 23 and As 75 NMR study of ant ferromagnetism and spin fluctuations in NaFeAs single crystals. *Physical Review* B,83, 132501.

[68] Hammes-Schiffer, S. (2017). (2017)A conundrum for density functional theory, *Science*, vol. 355, no. 2829.

[69] Giannozzi, P., Andreussi, O., Brumme, T., Bunau, O., Nardelli, M. B., Calandra, M, and Baroni, S. (2017). Advanced capabilities for materials modelling with Quantum ESPRESSO. *Journal of physics: Condensed matter*, 29, 46590.

[70] Moreno, J. R., Carleo, G., and Georges, A. (2020). Deep learning the hohenberg kohn maps of density functional theory. *Physical Review Letters*, 125,076402.

[71] Brockherde, F., Vogt, L., Li, L., Tuckerman, M. E., Burke, K., and Mller, K. R. (2017). Bypassing the Kohn-Sham equations with machine learning. *Nature communications*, 8, 1-10.

[72] Kazakov, Alexander D., Varvara M. Prokacheva, Filip Uhlk, Peter Koovan, and Frans AM Leermakers. (2021) "Computer modeling of polymer stars in variable solvent conditions:a comparison of md simulations, self-consistent field (scf) modeling and novel hybrid monte carloscf approach," *SoftMatter*, 17, 580591.

[73] Giannozzi, P., Baroni, S., Bonini, N., Calandra, M., Car, R., Cavazzoni, C, and Wentzcovitch, R. M. (2009). QUANTUM ESPRESSO: a modular and open source software project for quantum simulations of materials.*Journal of physics: Condensed matter*, 21, 395502.

[74] Barnes, T. A., Kurth, T., Carrier, P., Wichmann, N., Prendergast, D., Kent, P. R., and Deslippe, J. (2017). Improved treatment of exact exchange in Quantum ESPRESSO. *Computer Physics Communications*, 214, 52-58.

[75] Sharma, B. I. (2016, October). Basic concepts of Density Functional Theory: Electronic structure calculation. *In Journal of Physics*, 765,012004).

[76] Elliott, P., Furche, F., and Burke, K. (2009). 3 Excited States from Time Dependent Density Functional Theory. *Reviews in computationalchemistry*, 26, 91.

[77] Setyawan, W., and Curtarolo, S. (2010). High-throughput electronic bandstructure calculations: Challenges and tools. *Computational materials science*, 49, 299-312.

[78] Persson, Kristin. (2016). "Materials data on NaFeAs (sg:129) by materials project," vol. 2.